Demonstration of Frequency-Sweep Testing Technique Using a Bell 214-ST Helicopter

Mark B. Tischler, Jay W. Fletcher, Vernon L. Diekmann, Robert A. Williams, and Randall W. Cason

April 1987

NASA
National Aeronautics and
Space Administration

US ARMY
AVIATION
SYSTEMS COMMAND
AVIATION RESEARCH AND
TECHNOLOGY ACTIVITY

Demonstration of Frequency-Sweep Testing Technique Using a Bell 214-ST Helicopter

Mark B. Tischler,
Jay W. Fletcher, Aeroflightdynamics Directorate, U.S. Army Aviation Research and Technology
        Activity, Ames Research Center, Moffett Field, California

Vernon L. Diekmann,
Robert A. Williams,
Randall W. Cason, U.S. Army Aviation Engineering Flight Activity, Edwards Air Force Base,
        Edwards, California

April 1987

TABLE OF CONTENTS

LIST OF TABLES

LIST OF FIGURES

NOMENCLATURE

a_z vertical acceleration, positive downward, g

f frequency, Hz

G transfer function

G_{xx} input autospectrum

G_{xy} cross-spectrum

G_{yy} output autospectrum

h altitude, ft

$\dot{h}$ vertical velocity, positive upward, ft/sec

K gain

M_q pitch damping

M_u speed stability

p roll rate, deg/sec

q pitch rate, deg/sec

r yaw rate, deg/sec

s Laplace variable

T period, sec

T_h vertical axis time constant, sec

T_w window length, sec

V_a airspeed, knots

Z_w heave damping

β side-slip angle, deg

γ_{xy}^2 coherence function between variables x and y

δ_{LAT} lateral cyclic stick deflection, in.

δ_{LON} longitudinal cyclic stick deflection, in.

δ_{PED} pedals deflection, in.

δ_{COL} collective stick deflection, %

ζ damping ratio

θ pitch angle, deg

τ_e time delay, sec

τ_p phase-delay, sec

ϕ roll angle, deg

Φ_m phase margin, deg

Φ_1 phase at frequency at which phase-delay is evaluated, deg

$\Phi_{2\omega_{180}}$ phase at twice neutral stability frequency, deg

ψ yaw angle, deg

ω frequency, rad/sec

ω_{BW} bandwidth frequency, rad/sec (see definition in fig. 1)

ω_{GM} frequency at which gain margin is 6 dB, rad/sec

ω_{input} frequency of control input waveform, rad/sec

ω_{max} maximum frequency of control input waveform, rad/sec

ω_{min} minimum frequency of control input waveform, rad/sec

ω_n natural frequency, rad/sec

ω_1 frequency at which phase-delay is evaluated, rad/sec

ω_{135} frequency at which phase margin is 45 deg, rad/sec

ω_{180} neutral stability frequency, rad/sec

$1/T$ inverse time constant, rad/sec

DEMONSTRATION OF FREQUENCY-SWEEP TESTING TECHNIQUE USING A

BELL 214-ST HELICOPTER

Mark B. Tischler and Jay W. Fletcher
Aeroflightdynamics Directorate
U.S. Army Aviation Research and Technology Activity
Ames Research Center, Moffett Field, California

Vernon L. Diekmann, Robert A. Williams, and Randall W. Cason
U.S. Army Aviation Engineering Flight Activity
Edwards Air Force Base, Edwards, California

SUMMARY

A demonstration of frequency-sweep testing using a Bell 214ST single-rotor helicopter was completed in support of the Army's development of an updated MIL-H-8501A, and an LHX (ADS-33) handling-qualities specification. Hover and level-flight condition (V_a = 0 knots and V_a = 90 knots) tests were conducted in 3 flight hours by Army test pilots at the Army Aviation Engineering Flight Activity (AEFA) at Edwards AFB, CA. Bandwidth and phase-delay parameters were determined from the flight-extracted frequency responses as required by the proposed specifications. Transfer-function modeling and verification demonstrates the validity of the frequency-response concept for characterizing closed-loop flight dynamics of single-rotor helicopters--even in hover. This report documents the frequency-sweep flight-testing technique and data-analysis procedures. Special emphasis is given to piloting and analysis considerations which are important for demonstrating frequency-domain specification compliance.

1. INTRODUCTION

Research supporting the development of the LHX handling-qualities specification ADS-33 (ref. 1), an updated version of MIL-H-8501A (ref. 2), indicates the need for frequency-domain descriptions to characterize adequately the transient angular response dynamics of highly augmented combat rotorcraft (refs. 3 and 4). The proposed LHX criteria for short-term angular response are given in terms of two frequency-domain parameters: bandwidth (ω_{BW}) and phase-delay (τ_p). These quantities are determined directly from frequency-response plots of the on-axis angular responses to control inputs: θ/δ_{LON}, ϕ/δ_{LAT}, ψ/δ_{PED} as shown in figure 1.

Frequency-response plots such as figure 1 are easily generated from analytical models and are certainly useful design tools; however, a key concern in incorporating such descriptions in a specification is the practical problem of extracting frequency-responses from flight data for compliance testing. The frequency-sweep

DEFINITION OF PHASE DELAY

$$\tau_p = -\frac{\Phi_{2\omega_{180}} + 180°}{114.6\,\omega_{180}}$$

RATE RESPONSE-TYPES:

ω_{BW} is lesser of ω_{GM} and ω_{135}

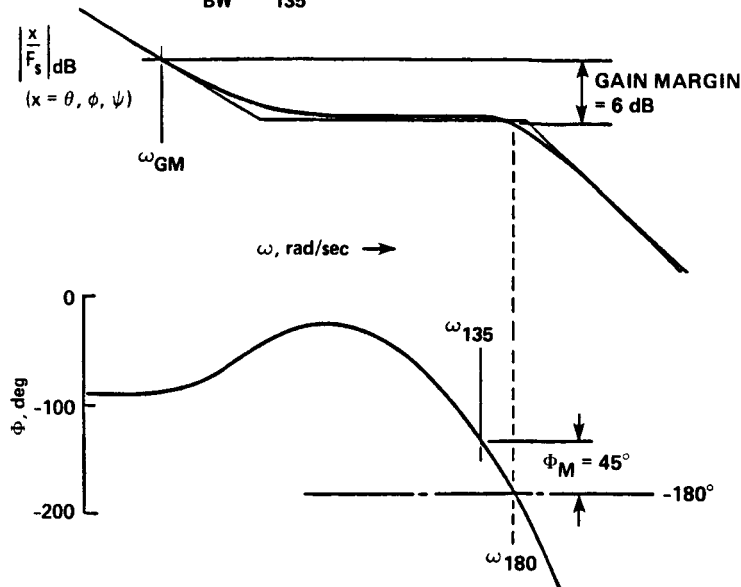**ATTITUDE RESPONSE-TYPES:**

$\omega_{BW} \equiv \omega_{135}$

Figure 1.- Definitions of bandwidth and phase delay.

method for obtaining frequency-responses from flight vehicles has been extensively demonstrated in fixed-wing aircraft (ref. 5), nonconventional aircraft (ref. 6), twin-rotor helicopters (refs. 7 and 8), and in piloted simulations of single-rotor helicopters (ref. 9). However, it has not been extensively demonstrated on conventional, single-rotor helicopters. Also, the test pilot and engineering staff of the U.S. Army Aviation Engineering Flight Activity (AEFA), who are responsible for conducting specification compliance testing of new vehicles, have little direct experience with the procedure.

To address these concerns, a joint program between the Army Aircrew-Aircraft Integration Division of the Aeroflightdynamics Directorate (Ames Research Center), and AEFA (Edwards AFB) was initiated. The primary objectives of this program were to:

1. Demonstrate and validate frequency-domain test techniques for a conventional, single-rotor helicopter.

2. Demonstrate that frequency-domain methods are easy to learn and apply in LHX specification-compliance testing.

3. Transfer frequency-domain testing and analysis technology to the U.S. Army testing facility (AEFA).

During the initial planning of this program, the intention was to use a fully instrumented UH-60 Blackhawk aircraft. However, the long grounding of this vehicle and the urgent need to complete the frequency-sweep demonstration test required the selection of an alternate vehicle. A modestly instrumented Bell 214-ST helicopter (which was then on loan to the AEFA facility) was selected (fig. 2). Frequency-sweeps were conducted at two flight conditions, V_a = 0 knots and V_a = 90 knots, to reveal testing and analysis differences for hovering and forward flight. The stability-and-control augmentation system (SCAS) was engaged for all of the tests to demonstrate the extraction of the end-to-end frequency response as is required by the LHX specification. Frequency-sweep control inputs and step control inputs were conducted in each control axis for both flight conditions. The total test time (including practice runs) was 3 flight hours.

This report documents the frequency-sweep flight-testing technique and data-analysis procedures. Special emphasis is on piloting and analysis considerations which are important for demonstrating frequency-domain specification compliance. Section 2 discusses the flight-test requirements for obtaining the specification parameters defined in figure 1. The overall testing-and-analysis approach is discussed in Section 3. The theoretical details are omitted in this report since they are extensively discussed in other publications (refs. 7,10,11). Section 4 describes the Bell 214-ST test vehicle, the on-board instrumentation, and the ground-support equipment. Section 5 summarizes the flight tests, with special emphasis given to key piloting problems and suggestions. Section 6 discusses in detail the analysis of the roll response in hover, and summarizes the results for the remaining axes (all of the analyzed data are presented in the appendixes). Based on present and previous flight tests, guidelines are given in Section 7 for
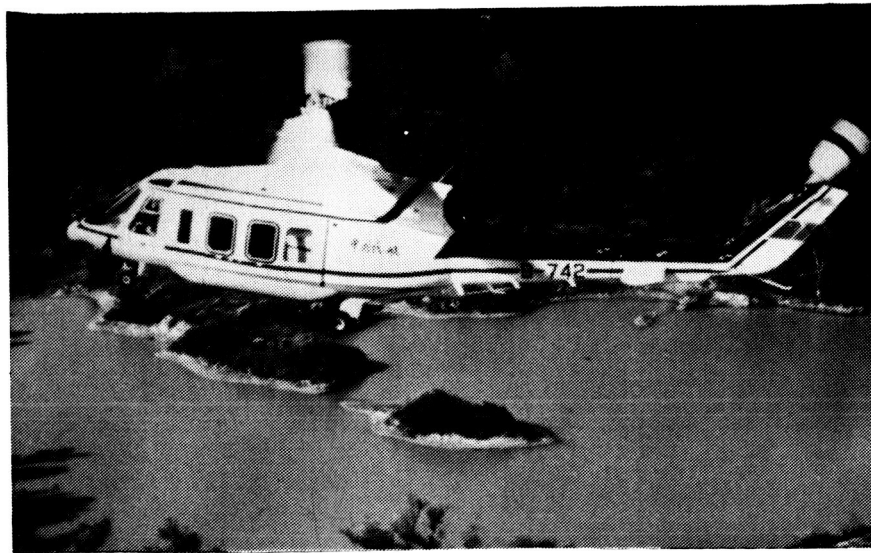

Figure 2.- The Bell 214ST helicopter.

obtaining high-quality results using the frequency-sweep method. Overall conclusions are presented in Section 8.

2. REQUIREMENTS FOR COMPLIANCE TESTING

The flight-test inputs and analyses methods are tailored to obtain the needed frequency-domain specification parameters of figure 1. Experience has shown that a good indentification of the angular response to pilot input must be obtained in the frequency range from below the bandwidth frequency to above twice the frequency that produces 180 deg of phase shift, or roughly:

$$0.5 \ \omega_{BW} \leq \omega \leq 2.5 \ \omega_{180} \tag{1}$$

The pilot-generated frequency-sweep input of figure 3 is effective in exciting the helicopter in the desired range. The range of excitation is determined by selecting the period of the lowest frequency input and the cycle rate of highest frequency input. However, since the objective of the test is to identify the frequency response, the required sweep range (eq. 1) is not accurately known beforehand. Therefore, a conservative guess is made based on simple analyses. Trial and repeat test procedures may be needed to improve the data quality in a particular frequency range. For the Bell 214 aircraft, the frequency range:

$$0.4 \ rad/sec \leq \omega_{input} \leq 12.0 \ rad/sec$$

was selected. This sets the low-frequency period and high-frequency cycle rate as follows:

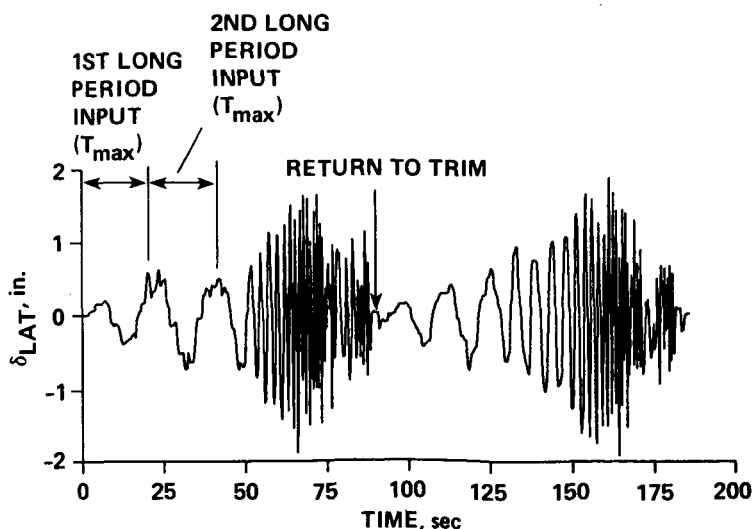$$T_{max} = \frac{2\pi}{\omega_{min}} = 16 \ sec$$

Figure 3.- Frequency sweep input.

4

$$f_{max} = \frac{\omega_{max}}{2\pi} = 2 \text{ Hz}$$

The limitations on achieving longer low-frequency periods are the relatively large attendant motions and off-axis coupling. High-frequency inputs are limited by the ability of the pilot to drive the conventional controllers, but are generally achievable up to about 4 Hz. In the Bell 214 tests, the maximum input frequency was restricted to about 2 Hz to avoid exciting the rotor pylon structural mode at $\omega = 12$ rad/sec. In the vertical axis, the period of the low-frequency input was increased to $T_{max} = 20$ sec to ensure good low-frequency identification. High-frequency inputs of the collective lever were achieved up to about 1.5 Hz.

With the low- and high-frequency inputs specified, the remaining parameter to be determined in figure 3 is the overall length of the run. Previous frequency-sweep testing experience on the XV-15 aircraft indicates that a 90-sec run is necessary to produce an even distribution of frequency content between the low- and high-frequency cycles. At least two complete 90-sec frequency sweeps are concatenated to increase the amount of data used in the spectral analysis and thus reduce the variance in the spectral estimates. To ensure that two good runs were obtained, three frequency-sweeps were executed consecutively in each axis. Following the frequency-sweep inputs for a specific axis, step inputs in that axis were obtained. These were used in the frequency-response verification study.

The need to accurately identify the frequency-response characteristics in the frequency range of equation 1 implies a number of important additional flight-test requirements. The instrumentation (sample rate and bandwidth) must be carefully selected so that its dynamic response has little effect on the identified overall dynamic response. The characteristics of the sensors and filters must be well known so that their effect can be incorporated in the analysis. Obtaining good quality data also requires that the flight tests be conducted during periods of minimum ambient wind and turbulence. Steady winds of less than 5 knots are desirable when the helicopter is in hover. Higher wind velocities are acceptable in forward flight if turbulence levels are light (roughly 1 to 2 knots). Measured response distortion resulting from recording equipment, sensor and filter dynamics, and atmospheric disturbances all degrade the precision and accuracy with which the real vehicle dynamics can be identified.

3. TESTING AND ANALYSIS APPROACH

The testing-and-analysis approach used in the present demonstration effort (fig. 4) closely follows the methods developed in the XV-15 program (refs. 7,10,11). However, the present study emphasized the demonstration of specification compliance rather than parameter identification.

The flight tests and a preliminary data analysis were conducted during a 2-day period, with the actual flight testing requiring about 3 hours of flight time.
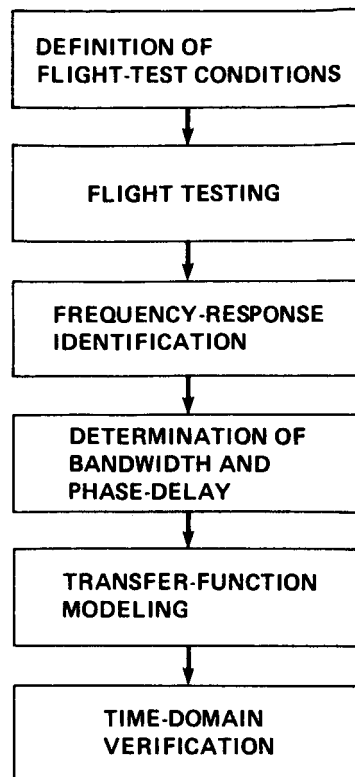
5

```
┌─────────────────────────┐
│ DEFINITION OF           │
│ FLIGHT-TEST CONDITIONS  │
└─────────────────────────┘
            │
            ▼
┌─────────────────────────┐
│ FLIGHT TESTING          │
└─────────────────────────┘
            │
            ▼
┌─────────────────────────┐
│ FREQUENCY-RESPONSE      │
│ IDENTIFICATION          │
└─────────────────────────┘
            │
            ▼
┌─────────────────────────┐
│ DETERMINATION OF        │
│ BANDWIDTH AND           │
│ PHASE-DELAY             │
└─────────────────────────┘
            │
            ▼
┌─────────────────────────┐
│ TRANSFER-FUNCTION       │
│ MODELING                │
└─────────────────────────┘
            │
            ▼
┌─────────────────────────┐
│ TIME-DOMAIN             │
│ VERIFICATION            │
└─────────────────────────┘
```

Figure 4.- Testing and analysis procedure.

Onboard pulse code modulation (PCM) flight data were transferred to the AEFA VAX 11/780 computer. A simple FORTRAN program was developed to reformat the flight data for input to the frequency-response identification program, FRESPID. The outputs from FRESPID are time history and frequency-response plots, and a tabular data file. Using these results and the specification definitions in figure 1, the bandwidth and phase-delay parameters were obtained. This completed the specification compliance-testing demonstration.

Besides demonstrating compliance testing, a second major objective was to demonstrate that frequency-response descriptions are valid for single-rotor helicopters. There was special concern over the validity of these linear decoupled descriptions for large motion dynamics in the hover flight condition. To address this issue, lower-order transfer-function models were extracted from the identified frequency responses. Then, the responses of the model and aircraft to step inputs were compared to verify the suitability of the identified models.

6

4. TEST VEHICLE AND SUPPORT EQUIPMENT

4.1 Vehicle Description

The Bell 214-ST is a medium weight, single teetering-rotor helicopter with a maximum gross weight of 17,500 lb. For the demonstration program, the vehicle was operated at 13,000 lb to minimize the possibility of over-torqueing the transmission during frequency sweeps in the collective axis. As previously mentioned, the entire test was conducted with the stability and control augmentation system (SCAS) engaged. This system has a 10% control authority and provides feedback and feedforward augmentation to enhance the vehicle's inherent stability and to shape the response to the pilot's stick inputs. The feedback loops (which use signals from rate gyros) provide attitude rate, and lagged-attitude rate compensation to improve the closed-loop damping and gust rejection. The active stabilator, which is in the rotor downwash, significantly increases the inherent pitch damping (M_q) and speed stability (M_u). The pitch-axis channel also has increased lead compensation in the feedback loops relative to the roll axis. These differences make the closed-loop pitch dynamics significantly more damped and at lower frequency than the roll dynamics. The command augmentation networks are roughly the same in the pitch, roll, and yaw axes. The networks add lag to the stick response which reduces control abruptness (and response bandwidth), thereby improving ride qualities.

4.2 Instrumentation

The test vehicle was instrumented with a full complement of rate and attitude gyros, and a vertical accelerometer. Pilot control positions and rotor rpm were also measured. The vehicle was equipped with an on-board PCM recorder which provided data at the relatively low sample rate of 31 Hz and maximum digital skews between adjacent channels of 15 msec. The instrumentation package was primarily intended for use in performance testing and was not ideally suitable for compliance frequency-sweep testing. Detailed information on the dynamic characteristics of the sensors and their filters was not available, so no correction for these effects was made to the data. As previously stated, a higher sample rate data-acquisition system which is carefully calibrated and documented is needed for actual compliance testing; however, for the present demonstration effort, the available instrumentation was felt to be adequate.

4.3 Ground Support Equipment

A telemetry (TM) downlink was established and maintained between the aircraft and the ground station during the entire test. Control positions and angular rates were monitored to coach the pilot during the frequency-sweep testing. Postflight data processing and analysis was conducted on the AEFA VAX 11/780 computer using the FRESPID program, which was readily adapted to available computer graphics. All frequency-response analyses were conducted at AEFA by their own on-site engineers.

7

Initial frequency responses for the hover and forward-flight condition were generated within a few hours after the completion of the flight tests. The output data from FRESPID were transferred to the Aeroflightdynamics Directorate (Ames Research Center) for the transfer-function identification and model verification phases of the study.

5. FLIGHT TESTS

5.1 Preflight Preparation

A key consideration in this demonstration program was that neither evaluation pilot had significant previous experience with the frequency-sweep testing method. A 1-hour briefing was conducted the day before the tests with the pilots and flight-test personnel to review the method. The briefings covered the basic sweep input form, instructions for off-axis regulation, and a short film showing frequency-sweeps on the XV-15 aircraft. Important aspects of frequency-sweep testing which were reviewed in this preflight meeting are summarized in Section 7.1.

A preflight briefing was conducted in the morning before the flight test by project pilot and co-pilot. The two test conditions (V_a = 0 knots, V_a = 90 knots) were selected to illustrate piloting and analysis problems in the hover and forward flight regimes while staying away from the edge of the operating envelope of the Bell 214-ST. Hovering tests were planned at 75 ft above ground level, to be free of ground effect. The flight-test card called for three "good" frequency-sweeps and two step inputs in each axis for both flight conditions. The operational limits of the aircraft were reviewed and maximum allowable excursions were established. For the hover flight condition, the maximum excursions from trim were ±10 deg in pitch attitude and ±20 deg in roll attitude; for the forward flight condition, ±30 deg in pitch attitude and ±45 deg in roll attitude.

5.2 Hover Tests

The hover tests were conducted first to take advantage of the low wind velocities which exist in the early hours of the day at Edwards. Wind conditions during the hover tests were 6-8 knots, which is somewhat higher than desirable. Some initial frequency-sweeps were conducted to practice the method and to develop the protocol between the pilot, co-pilot, and flight-test engineers. No data were taken during the practice runs. There was an initial tendency for the test pilot to make a discrete jump from low-frequency inputs to high-frequency inputs without the slowly increasing frequency content which is needed for good identification results. However, after a few practice runs and some real-time coaching from the ground and co-pilot, this tendency was rapidly overcome.

The pilots found that inputs to the vertical and yaw axes were the easiest to accomplish. They recommend that future tests be conducted in these axes first to

develop familiarity with the method before the more difficult roll and pitch sweeps are attempted. The pilots noted that significant pedal inputs were needed during the lateral sweeps and significant collective inputs were needed in longitudinal sweeps to maintain roughly constant reference conditions (Section 7.1). Noticeable vehicle resonance was reported for input frequencies exceeding 2 Hz. Discussions with the manufacturer indicated that this resonance was associated with the excitation of the rotor pylon structural mode. To reduce this effect, the pilot's input amplitude was reduced for frequencies exceeding 1.5 Hz. Step inputs were applied using a control jig (fixture) and were maintained until a roughly steady-state (rate) condition was achieved. Since the step inputs tended to produce larger off-axis responses than were encountered during the frequency-sweep testing, these inputs were restricted to smaller amplitudes. The hover flight test took 1.2 hr, including practice run, sweep, and step inputs.

5.3 Forward-Flight Tests

Forward-flight tests were conducted following the reloading of on-board flight tapes and refueling of the aircraft. When the forward-flight test began, the test pilots reported that the turbulence level was roughly ±1 knot which was characterized as "light turbulence." By the end of the forward flight tests, the pilots noted that the turbulence had increased to roughly ±2 knots which was characterized as "moderate turbulence." The pilots executed all of the frequency-sweeps in the forward flight condition with great ease and skill. They had no significant concerns other than the desire for cockpit control-position indicators. This would have been helpful for achieving more symmetrical input forms, especially in the collective axis. Frequency-sweeps and step inputs (including practice runs) for the forward flight condition took approximately 1 hour.

Useful guidelines for future frequency-sweep tests were compiled by the test pilots following the completion of the Bell 214-ST tests and are given in Section 7.2.

6. DATA ANALYSIS AND RESULTS

The analysis of the flight-test data was conducted in four steps:

1. Frequency-response identification from time histories.

2. Determination of bandwidth and phase-delay from frequency responses.

3. Transfer-function model identification.

4. Transfer-function model verification.

6.1 Frequency-Response Identification

This section discusses the analysis of the roll response in hover in detail and summarizes the results for the remaining axes. All flight-data plots and results are given in the Appendixes.

The proposed LHX handling qualities specification defines the short-term roll, pitch, and yaw <u>attitude responses</u> in terms of required bandwidth and phase-delay (see section 6.2.1) for hover. The vertical response is given in the time-domain. For the forward-flight condition, the frequency-response criteria are used for roll and pitch, while time-domain criteria are used for yaw and heave. In the present study, frequency-response identification was completed for all four on-axis responses in hover:

$$\text{Roll:} \quad \frac{p}{\delta_{LAT}} \text{ , deg/sec/in.}$$

$$\text{Pitch:} \quad \frac{q}{\delta_{LON}} \text{ , deg/sec/in.}$$

$$\text{Yaw:} \quad \frac{r}{\delta_{PED}} \text{ , deg/sec/in.}$$

$$\text{Heave:} \quad \frac{a_z}{\delta_{COL}} \text{ , g/in.}$$

In the forward-flight condition, the sideslip response, β/δ_{PED}, was also identified.

Frequency-response identification was completed using the angular rate variables (e.g., p,q,r) rather than the angular attitude variables (ϕ,θ,ψ) because the mid- and high-frequency content of the rate (or derivative) variables is greater. Therefore, this choice of signals is better suited for identification of the bandwidth and phase-delay parameters. When the identification of the low-frequency characteristics is more important, the attitude response variables are better suited for the analysis. The FRESPID program determines the required attitude responses from the rate responses by applying the simple $1/s$ conversion to the magnitude and phase curves. A comparison of the integrated rate and measured attitude data showed good agreement in the mid-frequency range.

6.1.1 <u>Responses in hover flight condition</u>- Analysis of the responses was initially done on each individual frequency-sweep. Each sweep was visually inspected for symmetry of input and output, and frequency content as determined from both the time history and frequency-response plots. The coherence function (discussed below) was used as the primary measure of identification quality. From this analysis of the individual frequency-sweep runs, the best 2-out-of-3 runs were selected for each axis. These two frequency sweeps were concatenated by the FRESPID program to produce an averaged, low-variance, frequency-response estimate.

Roll response. The two best lateral frequency sweeps are shown in the concatenated time history of figure 5. As previously discussed, each sweep is initiated with two low-frequency cycles, each having a period of 16 sec. After the initial low-frequency cycles, the control is moved at gradually increasing frequency for the maximum total run length of 90 sec. Notice that at low frequency, the input magnitude is roughly 0.75 to 1.0 in., while the mid-frequency inputs are closer to 1.5 in. At high frequencies, the input amplitudes are reduced to minimize the excitation of the rotor pylon resonance.

The input autospectrum ($G_{\delta_{LAT}\delta_{LAT}}$) in figure 6 displays the frequency distribution of the concatenated lateral stick sweeps. The frequency-sweep is seen to produce nearly constant input power in the frequency range of 0.2-7.0 rad/sec. The spectral content below the minimum average input frequency of $\omega = 0.4$ rad/sec ($T_{min} = 16$ sec) results from the various nonsinusoidal low-frequency input signal details. At high frequency, the reduced autospectrum reflects the deliberate reduction in input amplitude. Expanded time-history plots of the frequency sweep inputs indicate that the pilots could comfortably generate sizable inputs up to a frequency of about 4 Hz.
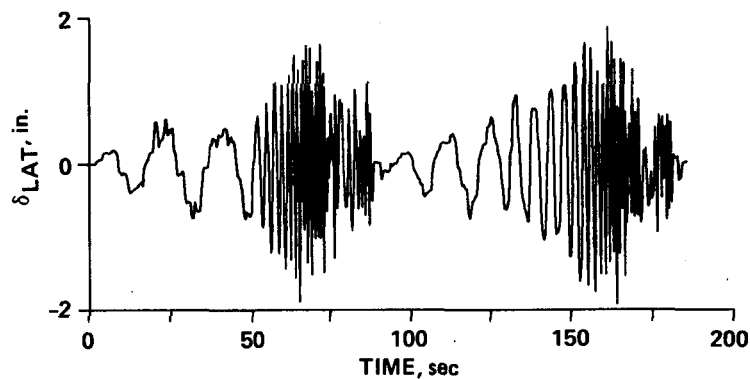
Figure 5.- Lateral stick frequency sweeps in hover.
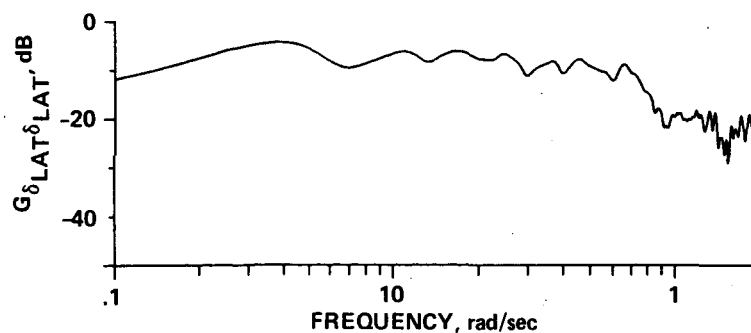
Figure 6.- Lateral stick input autospectrum in hover.

11

The concatenated roll rate responses for these two frequency sweeps are shown in figure 7. The maximum roll rate is about ±15 deg/sec, with somewhat lower values for low and high frequency inputs. The corresponding output autospectrum G_{pp} (fig. 8) shows that the roll rate excitation is roughly constant in the frequency range of 0.3-2.0 rad/sec (the closed-loop bandpass) and drops off thereafter. The peak in the response at $\omega = 11.9$ rad/sec is due to the excitation of the rotor-pylon mode. The output autospectrum drops sharply for frequencies below $\omega = 0.1$ rad/sec because there is little pilot input power at these frequencies and also because of the choice of processing windows (see section 7.4).

The roll-rate response to lateral stick (p/δ_{LAT}) is shown in figure 9. At the higher frequencies, the response exhibits a K/s characteristic which indicates that a roll acceleration results from a lateral stick input. The presence of the rotor-pylon mode at $\omega = 11.9$ rad/sec is also seen in figure 9. At very low frequencies, the roll rate is significantly reduced because of the large lateral velocity perturbations and associated wash-out in roll-rate response caused by the vehicle's inherent dihedral stability.
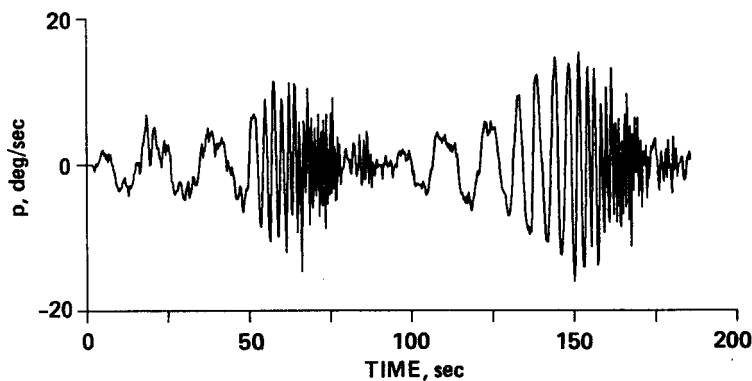
Figure 7.- Roll rate during lateral stick frequency sweeps in hover.
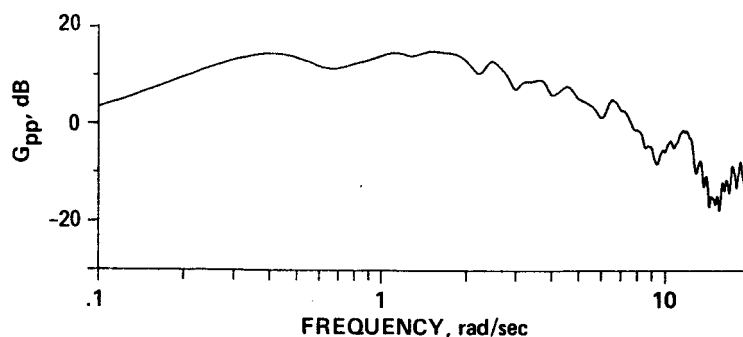
Figure 8.- Roll rate output autospectrum in hover.

12
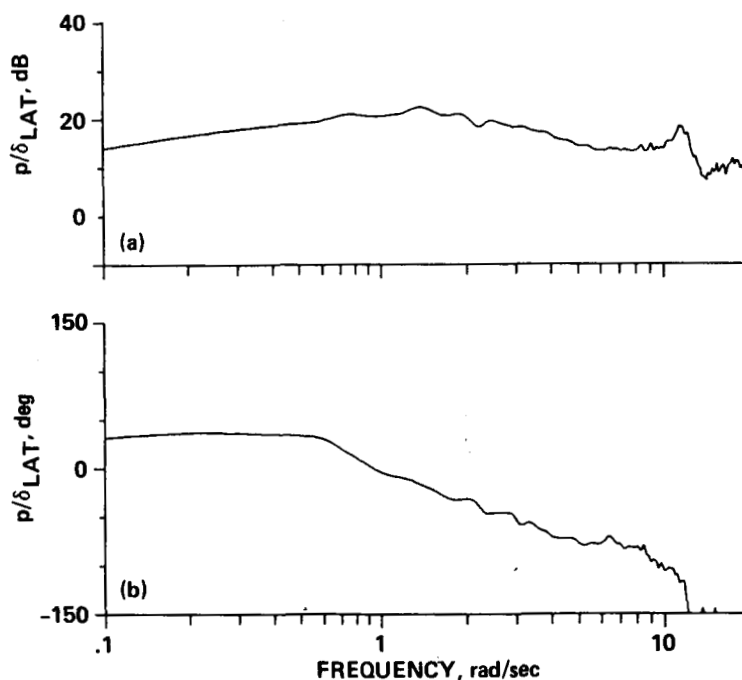
Figure 9.- Roll rate response to lateral stick in hover. (a) Magnitude; (b) phase.

The quality of the identified frequency response is assessed from the coherence function $\gamma^2_{\delta_{LAT}p}$ shown in figure 10. When the coherence function is greater than about 0.8 and does not oscillate, the identified frequency-response is considered to be sufficiently accurate. However, when the coherence function rapidly drops below the 0.8 level or sharply oscillates (as it does near $\omega = 12.0$ rad/sec, fig. 10), reduced accuracy in that frequency range is indicated. Common sources of reduced coherence are:
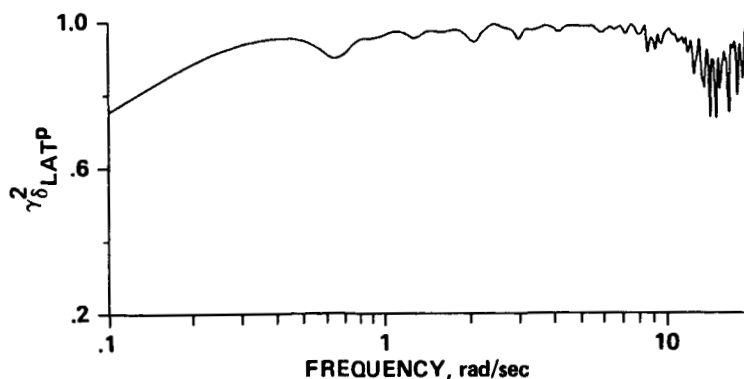
Figure 10.- Coherence function for roll rate response to lateral stick in hover.

1. Atmospheric turbulence
2. Excessive off-axis inputs
3. Sensor noise
4. Insufficient excitation of the vehicle
5. Significant nonlinearities

The best two-out-of-three frequency sweeps are chosen based on a desire to have a strong coherence function for the individual runs in the frequency range in which the bandwidths and phase-delays are calculated (eq. 1).

Figure 10 shows that the two concatenated frequency sweeps yield a good frequency response identification in the range of 0.2-12.0 rad/sec. For frequencies outside of this range, reduced coherence and oscillation of coherence are strong indications of reduced spectral accuracy.

The desired final plot of roll-attitude response to lateral stick (shown in fig. 11) is obtained from the roll-rate response by the integration: $\theta = p/s$. With this final frequency-response in hand, the next step is the extraction of the bandwidth and phase-delay parameters. Before this procedure is discussed, however, frequency-response identification results for the remaining axes will be briefly presented.
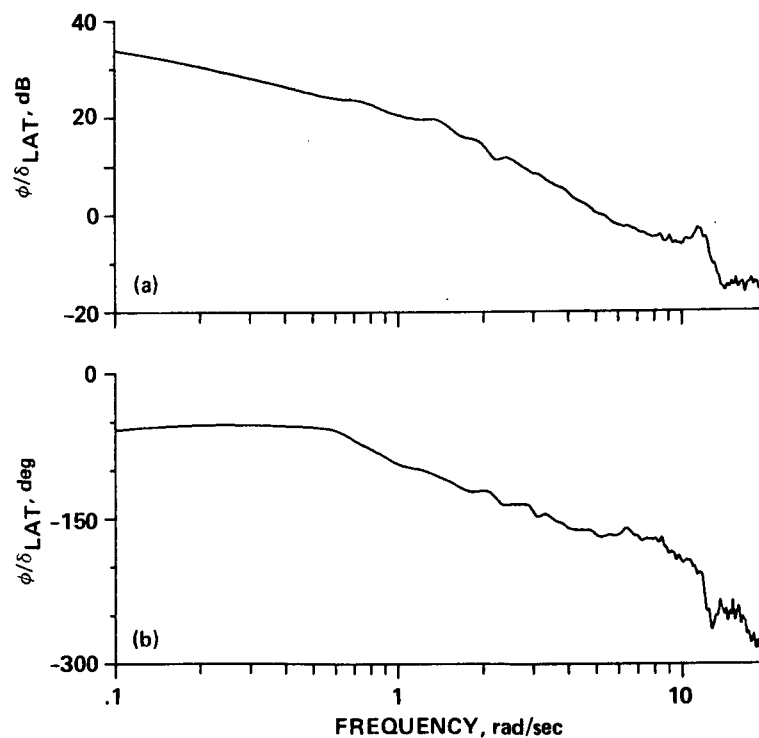
Figure 11.- Roll attitude response to lateral stick in hover. (a) Magnitude; (b) phase.

14

<u>Pitch response</u>. The difficulty in generating large low-frequency input signals in the pitch axis, in addition to the greater than desirable wind velocity, resulted in poor pitch response identification at the lowest input frequencies. However, the coherence function $\gamma^2_{\delta_{LON}q}$ (see fig. A14*) indicates good identification in the range of 0.5-12.0 rad/sec, which is satisfactory for showing specification compliance. The rotor pylon mode at $\omega = 12$ rad/sec (fig. A13) is again apparent. The pitch rate response to longitudinal stick displays a dominant mode (corner frequency) at $\omega = 1$ rad/sec with a rapid roll-off in response above this frequency. Compared to the dominant roll-response mode at about $\omega = 2$ rad/sec (fig. 9), the pitch-response is seen to be much more sluggish. This difference between pitch and roll responses reflects the difference in the SCAS configuration and the effect of the active horizontal stabilator as described earlier.

<u>Yaw response</u>. The regular and symmetric pedal frequency sweeps in hover (fig. A17) resulted in excellent identification of the yaw-rate response in the frequency range of 0.25-9.0 rad/sec (fig. A22). The yaw rate transfer function (fig. A21) exhibits a first-order response characteristic.

<u>Heave response</u>. Similarly smooth and regular collective inputs (fig. A25) produced excellent identification of the heave response in the frequency range of 0.2-10.0 rad/sec (fig. A30). The reduced lowest-frequency input for heave ($T_{max} = 20$ sec) is seen to improve the low-frequency identification. Also, the processing windows were optimized to improve the spectral identification in the lower-frequency range (section 7.4). The magnitude and phase characteristics in the vertical axis (fig. A29) indicate a low frequency for the dominant heave response mode $1/T_h = 0.1$ rad/sec. The verification study presented in section 6.4 supports this result. Estimates of heave damping for the Bell 214 based on simple momentum theory approximations suggest that the <u>small perturbation value</u> should be roughly $1/T_h = Z_w = -0.3$ rad/sec. The difference between the calculated and identified values of heave damping may be a result of the large rotor loading (reference condition) changes which occur during the frequency sweep. Similar reductions in effective heave damping determined from large-motion frequency sweep responses have also been observed in analyses conducted on the NASA Ames CH-47 aircraft (ref. 12).

6.1.2 <u>Responses in forward flight condition</u>- The smooth and regular frequency sweeps obtained for all of the axes in the forward flight condition resulted in improved spectral identification compared to the hover condition.

<u>Roll response</u>. The two best lateral stick frequency sweeps are shown in figure 12. Notice the improved wave form compared to the hover case of figure 5. The first frequency-sweep is seen to have better mid-frequency content, while the second frequency-sweep has better low-frequency content. By concatenating these two runs, excellent frequency response identification is achieved in the frequency range of

---

*The appendixes consist of a complete compendium of the results. Only representative samples are discussed in the text.
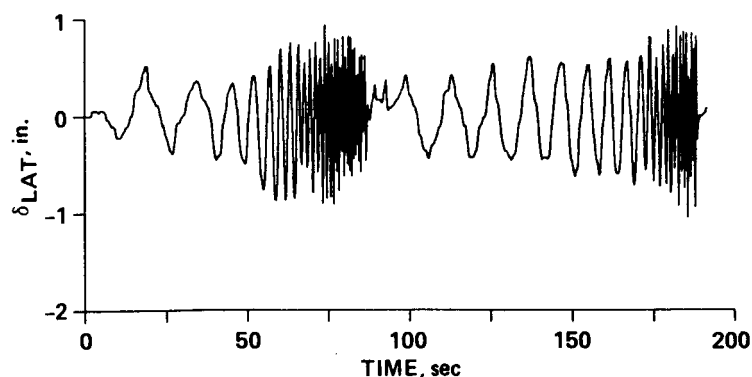
Figure 12.- Lateral stick frequency sweeps in forward flight.

0.3-12 rad/sec (fig. B6). As before, the roll-angle response needed for determining bandwidth and phase-delay is determined from the roll-rate response by applying a 1/s integration factor.

Pitch response. The improved low-frequency longitudinal stick inputs and more evenly distributed input frequency content for the forward-flight condition sweeps (see fig. B9) compared to those in hover (see fig. A9) yielded better low- and mid-frequency pitch response identification. Strong coherence was achieved in the frequency range of 0.3-5 rad/sec (fig. B14). Oscillations in the coherence function for frequencies greater than 5.5 rad/sec indicate reduced spectral accuracy. This is due to the reduction in magnitude of pilot inputs as the pylon structural mode is approached, and the moderate level of turbulence which was apparent during the forward flight tests.

Yaw response. For the forward-flight condition, identification of the yaw-rate and sideslip responses to pedal inputs was conducted. As in the other control axes during this flight condition, the pedal inputs were smooth and regular with nearly constant input amplitude (fig. B17). The resulting yaw-rate frequency response (fig. B21) has good coherence in the frequency range from 0.2-8.0 rad/sec (fig. B22). Accurate identification of the sideslip response was achieved only in the frequency range of 0.2-3.5 rad/sec (fig. B30). This occurred because the side-slip variable is a lower-order derivative compared to yaw rate. Therefore, the sideslip response rolls off 20 dB/decade faster than the yaw response. The rapid sideslip response attenuation causes reduced signal-to-noise content at the higher frequencies which is reflected in a much earlier drop in the coherence function.

Heave response. The coherence for heave-response identification is excellent for the entire frequency range of 0.2-20.0 rad/sec (fig. B38). However, the availability of only one good heave sweep (fig. B33) means 50% less averaging for this case as compared to hover. Therefore, the error variance increases by roughly 40% (ref. 11). Based on the input, output, and cross spectral plots, accurate identification is achieved in the frequency range of 0.2-10.0 rad/sec. The magnitude and phase plots for vertical acceleration response to collective (fig. B37) show

significantly increased heave damping for the forward flight condition relative to the hover case. This would be expected since the perturbation value of the heave damping derivative increases with speed. Also, the variations in rotor loading are much smaller in the forward-flight condition than in hover (because of the larger reference freestream velocity).

6.2 Determination of Bandwidths and Phase-Delays

At this point, all of the required frequency responses have been identified. The next step in the compliance demonstration procedure is the extraction of the bandwidth and phase-delay parameters from the frequency responses.

6.2.1 Definitions of Bandwidth and Phase-Delay- The bandwidth and phase-delay parameters needed for demonstration of specification compliance are defined in terms of the attitude frequency-response in figure 1. The bandwidth, ω_{BW}, for a rate-response-type system (like the Bell 214-ST) is the lower of two frequencies: one, ω_{GM}, based on a gain margin of 6 dB; and the other, ω_{135}, based on a phase margin of 45 deg. The bandwidth for an attitude response type system is defined to be ω_{135}.

The phase-delay, τ_p, is defined by:

$$\tau_p = \frac{-\Phi_1 - 180^\circ}{57.3\ \omega_1} \tag{2}$$

where Φ_1 is the phase at the frequency ω_1. When equation 2 is evaluated at twice the neutral stability frequency ($\omega_1 = 2\omega_{180}$) the equation takes on the form shown in figure 1:

$$\tau_p = -\frac{\Phi_{2\omega_{180}} + 180^\circ}{114.6\ \omega_{180}}$$

where $\Phi_{2\omega_{180}}$ is the phase at twice the ω_{180} frequency. It can be seen from the form of equation 2 that this parameter is a two-point measure of the rate at which the phase curve rolls off near ω_{180}, one point being fixed at ω_{180}.

The phase-delay can also be thought of as an approximation of the equivalent time delay, τ_e, which would result from fitting a second-order transfer function with time delay

$$G(s) = \frac{Ke^{-\tau_e s}}{s^2 + 2\zeta\omega_n s + \omega_n^2}$$

17

to the attitude frequency-response data. To the extent that the rolloff in phase beyond the -180 deg frequency can be attributed to the time delay only, the phase of $G(s)$ can be approximated by:

$$\Phi_1 = -180^\circ - 57.3\ \tau_p \omega_1 \qquad (\omega_1 > \omega_{180}) \qquad (3)$$

When equation 3 is solved for τ_p, we obtain equation 2. As the selected value of ω_1 approaches infinity, the phase-delay closely approximates the time delay, and therefore does not depend on the choice of ω_1. This is because the contribution of the second-order dynamics to the phase approaches -180 deg and the assumption that the phase rolloff is entirely due to the time delay becomes more valid. However, when ω_1 is close to ω_{180}, the phase-delay is not a good approximation of the time delay. This is because the lower-order dynamics still have a significant effect on the phase curve, causing it to vary nonlinearly with frequency and making the phase-delay value dependent upon the selected frequency ω_1. This is illustrated in figure 13 which shows a linear plot of the phase curve of the second-order system with time delay

$$G(s) = \frac{e^{-0.1s}}{s^2 + s + 1} \qquad (4)$$

The nonlinear phase response caused by the lower-order dynamics ($\zeta = 0.5$, $\omega_n = 1$ rad/sec) near $\omega_{180} = 3.3$ rad/sec can readily be seen. A calculation of τ_p in the linear region of the curve, at a frequency well above twice the ω_{180} frequency ($\omega_1 = 20$ rad/sec) yields a phase-delay of $\tau_p = 0.099$ sec. This is indeed very close to the value of the time delay, $\tau_e = 0.1$ sec. Calculating τ_p at $\omega_1 = 2\omega_{180} = 6.6$ rad/sec, however, yields a phase-delay of 0.077 sec. Therefore, to ensure consistent comparisons of phase-delay values with the specification and those calculated from other flight conditions and aircraft, phase-delays should always be calculated at the same frequency ($\omega_1 = 2\omega_{180}$). The numerical difference between the phase-delay and the time-delay parameters is not of concern since the specification
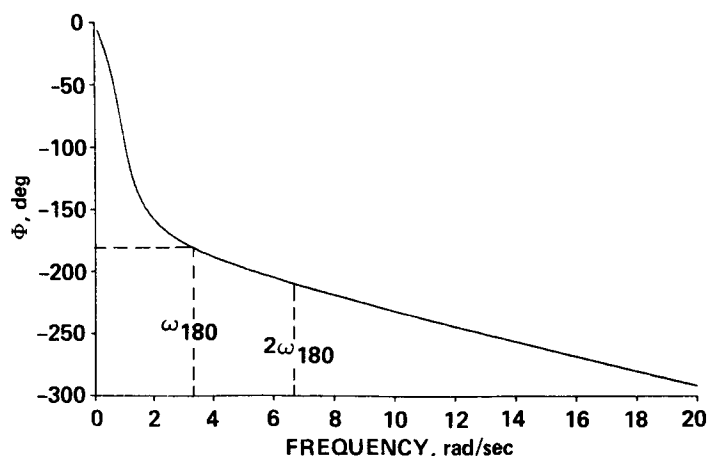
Figure 13.- Phase response of equation 4 on a linear frequency plot.

is based on correlation of handling-qualities data with the <u>phase-delay</u> parameter only.

Phase curve roughness caused by low coherence data and the effects of dynamics above the bandwidth frequency can make it difficult to determine the $\omega = \omega_{180}$ and $\Phi = \Phi_{2\omega_{180}}$ points. In such cases, it is useful to plot the phase data on a linear frequency scale and apply a least-squares fit in the roughly linear region. This technique is illustrated below for the roll response in hover.

6.2.2 <u>Results for hover flight condition</u>- Table 1 summarizes the bandwidths and phase-delays calculated for all axes during both flight conditions.

<u>Roll axis</u>. The frequency-response for roll attitude due to lateral stick in hover previously shown in figure 11 is repeated in figure 14. Because the roll response is a rate-type response, the bandwidth is the lesser of the ω_{GM} and ω_{135} frequencies. Figure 14 shows that the bandwidth is $\omega_{BW} = \omega_{135} = 2.40$ rad/sec which is rather large compared to the bandwidths in the other axes (table 1). The second-order response in roll attitude causes the ω_{180} and $2\omega_{180}$ frequencies to also be high ($\omega_{180} = 9$ rad/sec and $2\omega_{180} = 18$ rad/sec). As seen in figure 14, the phase characteristics above $\omega = 11$ rad/sec are heavily influenced by the rotor-pylon mode at $\omega = 11.9$ rad/sec. Furthermore, the coherence function is erratic at $2\omega_{180} = 18$ rad/sec so at this frequency the data are unusable.
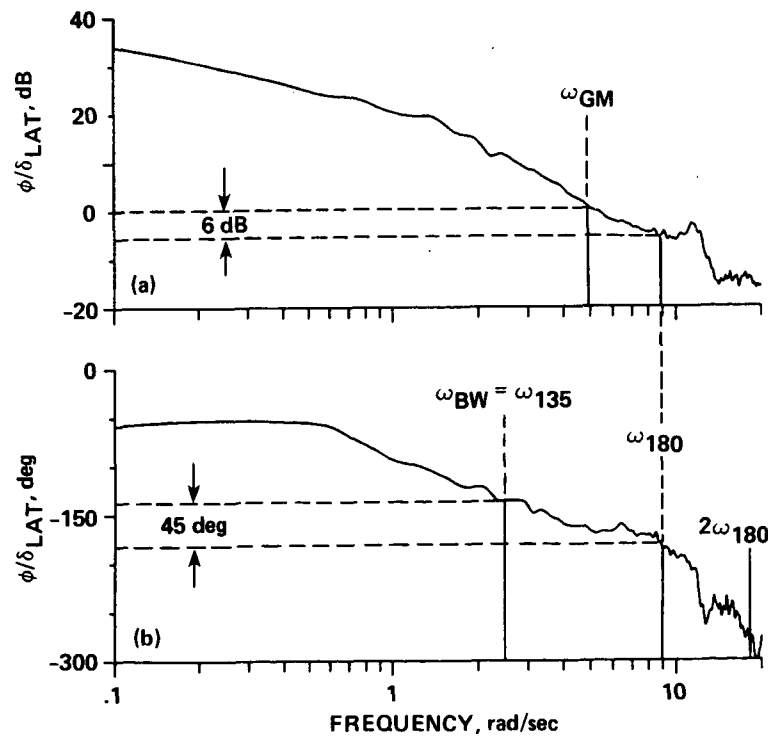
Figure 14.- Roll attitude response to lateral stick in hover. (a) Magnitude;
(b) phase.

19

TABLE 1.- BANDWIDTHS AND PHASE DELAYS FOR HOVER AND FORWARD FLIGHT

Hover			Forward flight		
Axis	Bandwidth (rad/sec)	Phase delay (sec)	Axis	Bandwidth (rad/sec)	Phase delay (sec)
Roll	2.4	0.085	Roll	2.6	0.098
Pitch	1.1	0.24	Pitch	1.3	0.27
Yaw	1.5	0.048	Yaw	2.2	0.082
Heave	0.11	0.12	Sideslip	1.1	0.16
			Heave	0.43	0.15

Further insight can be gained by displaying a linear plot of phase vs. frequency (fig. 15). As figure 15 shows, the rotor-pylon mode at $\omega = 11.9$ rad/sec has destroyed the linear phase rolloff in the region of $\omega > 11$ rad/sec. Using the raw data would result in a phase-delay that is not representative of the phase rolloff near $\omega = \omega_{180}$. A more representative value is obtained by constructing a linear extension of the phase curve from the linear region near the neutral stability frequency to $\omega = 2\omega_{180}$. In figure 15, this line is determined by applying a least squares fit to the phase data in the linear region between the frequencies of 8 and 11 rad/sec. The value of the phase **which would have occurred** at $\omega = 2\omega_{180}$ had the phase curve continued to roll off linearly can then be taken from this

$$\tau_p = -\left[\frac{(-268 + 180)}{(114.6)(9.0)}\right] = 0.085 \text{ sec}$$
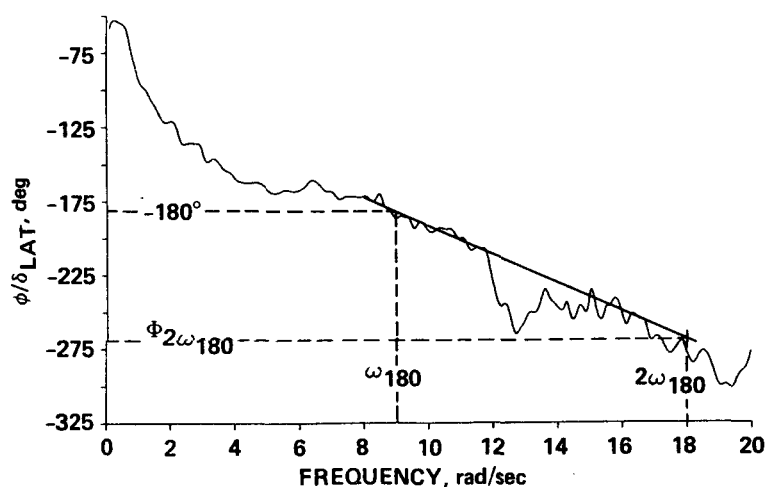
Figure 15.- Linear frequency plot of phase of roll rate response to lateral stick in hover.

20

line. The constructions of figure 15 yield a phase-delay of $\tau_p = 0.085$ sec. This method is also useful for cases when the coherence is poor at high frequencies even when structural modes are not present.

Other axes. As was mentioned earlier, the pitch axis is much more heavily damped than the roll axis which gives the pitch response a much lower bandwidth ($\omega_{BW} = 1.1$ rad/sec; table 1; and fig. A13). Also, the response is roughly third order in the frequency-range of interest. This lowers the ω_{180} and $2\omega_{180}$ frequencies considerably compared to the roll axis, and places the phase-delay calculation in a frequency-range of high coherence well below the pylon mode. The phase-delay calculation is now performed in a frequency-range where the closed-loop aircraft dynamics are still significant and the phase curve is <u>not linear</u>. Therefore, the phase-delay cannot be considered an approximation of the time delay, although it is still representative of the phase rolloff near the neutral stability frequency.

The frequency response for vertical position response to collective in hover is shown in figure A33. The bandwidth <u>cannot be determined</u> from the raw flight response at $\phi_m = 45$ deg because high coherence data are not available at a low enough frequency ($\omega < 0.1$ rad/sec). A first-order transfer function fit of the response (section 6.3) places the dominant mode at $1/T_h = 0.114$ rad/sec which indicates a bandwidth of $\omega_{BW} = 1/T_h = 0.114$ rad/sec.

6.2.3 <u>Results for forward flight condition</u>- The phase-delay calculation for the roll response in forward flight requires the application of the least-squares technique as described previously for the roll response in hover. Also, as in the pitch response in hover, the phase-delay calculations for the pitch and yaw axes in forward flight are performed at low frequencies and are indicative of the closed-loop aircraft dynamics rather than high-frequency dynamics. A least-squares fit of the heave response phase curve in forward flight is helpful for determining the phase value $\phi_{2\omega_{180}}$.

6.2.4 <u>Observations</u>- Reference to table 1 shows that the phase-delays for the roll, pitch, and heave axes are essentially unaffected by flight condition. This is because the dynamics they reflect (i.e., rotor and SCAS responses) are roughly invariant with flight speed.

The bandwidths in the pitch and roll axes are unchanged between hover and forward flight. Although the open-loop dynamics in these axes change substantially with flight condition, the augmentation in the pitch and roll axes ensures constant closed-loop dynamics.

The dynamics of the unaugmented heave and lightly augmented yaw axes change substantially between hover and forward flight. This is reflected in significant bandwidth changes.

6.3 Transfer-Function Model Identification

The objective of the transfer-function identification study was to derive closed-form models which could be used to prove the validity of the frequency-response concept for characterizing closed-loop <u>flight dynamics</u> of single-rotor helicopters. Therefore, the model identification is restricted to the frequency range which <u>excludes the rotor pylon resonance</u>, and which is within the accurate identification frequency range as determined from the coherence function plots. Based on these restrictions, the frequency range is selected for transfer-function model fitting in each axis and flight condition (table 2).

The next step is to determine the appropriate model order for each response. An appropriate transfer-function representation for the purposes of this study is one that accurately models the dominant, on-axis, <u>closed-loop</u> responses (the off-axis responses and nearly cancelled modes are not considered). Therefore, the minimum order transfer function is selected which yields a reasonable representation of the data within the frequency-ranges defined in table 2.

TABLE 2.- FREQUENCY RANGES FOR TRANSFER FUNCTION FITTING

	Hover			Forward flight	
Axis	ω_{min} (rad/sec)	ω_{max} (rad/sec)	Axis	ω_{min} (rad/sec)	ω_{max} (rad/sec)
Roll	0.2	8.0	Roll	0.3	8.0
Pitch	0.5	8.0	Pitch	0.3	5.5
Yaw	0.2	9.0	Yaw	0.2	8.3
Heave	0.2	5.5	Sideslip	0.2	3.5
			Heave	0.2	8.0

6.3.1 <u>Results</u>- The derived lower-order transfer function models for each axis and flight condition are summarized in table 3. Comparisons of the aircraft and model frequency-responses for all cases are illustrated in appendixes A and B.

The following second-order transfer function was found to adequately reflect the closed-loop roll-attitude responses in the appropriate frequency-ranges (table 2) for both the hover and forward-flight conditions:

$$\frac{\phi}{\delta_{lat}} (s) = \frac{K e^{-\tau e^{s}}}{(s + 1/T_1)(s + 1/T_2)} \qquad (5)$$

22

TABLE 3.- IDENTIFIED TRANSFER FUNCTIONS FOR HOVER AND FORWARD FLIGHT†

Hover	Forward flight
$\dfrac{\phi}{\delta_{LAT}} = \dfrac{31.60\ e^{-0.041s}}{(0.49)(2.30)}$	$\dfrac{\phi}{\delta_{LAT}} = \dfrac{34.31\ e^{-0.077s}}{(0.52)(2.66)}$
$\dfrac{\theta}{\delta_{LON}} = \dfrac{39.16\ e^{-0.0s}}{(0.77)[0.74,1.30]}$	$\dfrac{\theta}{\delta_{LON}} = \dfrac{50.09\ e^{-0.056s}}{(0.97)[0.83,1.43]}$
$\dfrac{r}{\delta_{PED}} = \dfrac{33.78\ e^{-0.087s}}{(1.78)}$	$\dfrac{r}{\delta_{PED}} = \dfrac{22.55s(3.61)e^{-0.115s}}{(0.38)[0.54,2.75]}$
	$\dfrac{\beta}{\delta_{PED}} = \dfrac{44.79(1.79)e^{-0.355s}}{(0.38)[0.54,2.75]}$
$\dfrac{\dot{h}}{\delta_{COL}} = \dfrac{0.17\ e^{-0.173s}}{(0.11)}$	$\dfrac{\dot{h}}{\delta_{COL}} = \dfrac{0.20\ e^{-0.190s}}{(0.47)}$

Phase lag caused by high-frequency dynamics such as the rotor, actuators, and structural modes is accounted for by the time delay. For the hover condition, this model was fit to the roll-attitude frequency response shown in figure 11 yielding the following parameters:

$$K = 31.6\ \text{deg/sec}^2/\text{in}.$$

$$\tau_e = 0.041\ \text{sec}$$

$$1/T_1 = 0.49\ \text{rad/sec}$$

$$1/T_2 = 2.30\ \text{rad/sec}$$

---

†Shorthand notation: $[\zeta, \omega]$ implies $s^2 + 2\zeta\omega s + \omega^2, \zeta$ = damping ratio, ω = undamped natural frequency (rad/sec); and $(1/T)$ implies $s + (1/T)$, rad/sec.

Figure 16 shows that the extracted model fits the data well in the frequency range of concern (0.3-8.0 rad/sec). An analytical study of the roll-axis dynamics indicates that the slight divergence of the model from the data in the frequency range from 6-10 rad/sec could be due to SCAS compensation dynamics which are ignored using the simple model of equation 5. As expected from the second-order form of equation 5, the bandwidth and the dominant mode $(1/T_2)$ are nearly equal $(\omega_{BW} = 2.40 \cong 1/T_2 = 2.30)$.
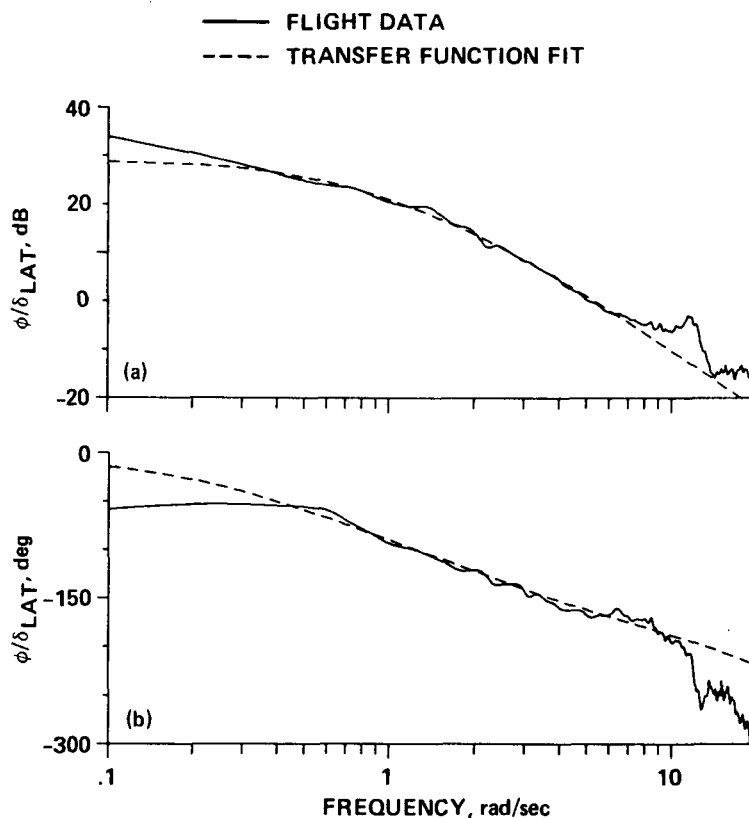
Figure 16.- Transfer function model for roll attitude response to lateral stick in hover. (a) Magnitude; (b) phase.

Third-order models (table 3) are required to characterize the closed-loop pitch dynamics in the appropriate frequency-ranges (table 2) for both hover and forward flight. As was mentioned earlier, the stabilator contributes to the pitch-axis dynamics, making this response fundamentally different from the roll response.

The closed-loop yaw response to pedals in hover is well characterized by a first-order model. The same is true of the unaugmented heave-axis dynamics in both hover and forward flight (table 3).

The yaw rate and side-slip angle responses to pedal in forward flight are characterized by third-order transfer functions. These responses share the same inherent dynamic modes; therefore, commonality of their transfer function

denominators must be enforced (ref. 11). This requirement is satisfied by simultaneously fitting the two responses (table 3).

6.3.2 <u>Observations</u>- The time delays of the fitted transfer functions are roughly unaffected by flight condition which is consistent with previous phase-delay results (table 1). Since time delays and phase-delays are calculated differently their values are not necessarily equal, but the trends in their values are similar as they should be. Both parameters (τ_p and τ_e) are measures of phase rolloff at high frequency. The large time delay in the sideslip transfer-function model accounts for the slow response of the sideslip angle measuring vane.

6.4 Transfer-Function Model Verification

The ability of simple transfer-function models to predict the time-domain response characteristics was tested by comparing the aircraft and model responses to step inputs. This input was selected for the verification study to show the robustness of the extracted models in predicting response characteristics to input forms other than the frequency-sweep form used in the identification process. However, the step input has high-frequency spectral content which excites aircraft modes outside of the transfer-function models' range of applicability (0.2-8.0 rad/sec, table 2) (ref. 12). Most important is the unwanted excitation of the rotor-pylon mode resonance at ω = 11.9 rad/sec. The input and output flight data are, therefore, low-pass filtered to attenuate their spectral content for frequencies beyond ω = 8 rad/sec. The <u>filtered</u> step input flight data are then used to drive the transfer-function model for comparison with the <u>filtered</u> output flight data. The low-order transfer-function model (eq. 5) and filtered aircraft roll-rate responses to a filtered lateral stick-step input are compared in figure 17.

Notice that the aircraft is well trimmed so that the match between the model and flight data initial conditions is good. The model closely predicts both the slope of the initial response and the subsequent course of the response to the constant input indicating that it is valid for a wide range of input frequencies. The error in predicted peak response is probably due to roll/yaw coupling which is ignored in the model (eq. 5). Overall, however, a good modeling of the helicopter dynamics by a low-order transfer function is obtained.

Comparisons of the aircraft and model responses to step inputs for all axes and flight conditions are illustrated in the appendixes. The matches are generally very good. Two exceptions are the pitch and yaw responses in hover (figs. A16 and A17, respectively) which show discrepancies developing beyond 7.5 sec. These are thought to be due to gusts. Another discrepancy occurs in the heave response to a sharp collective stick input in hover (fig. A32). The acceleration overshoot caused by the inflow dynamics is not modeled by the simple first-order transfer function form (ref. 12). Notice, however, that the response to more gradual inputs toward the end of the time history is accurately modeled.

The close matching of the model and aircraft step-responses in all axes and flight conditions indicates that a good, robust model of the vehicle dynamics has

25
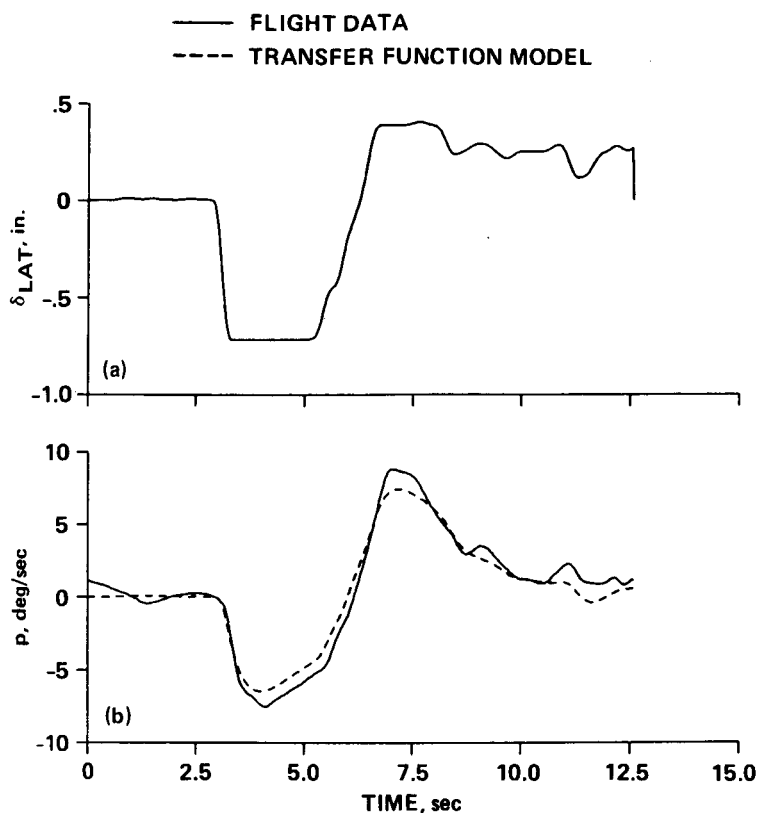
Figure 17.- Comparison of filtered aircraft response and transfer function model response to a filtered lateral stick step input in hover. (a) Lateral-stick input; (b) roll rate.

been achieved. Most important is the broader conclusion that linear, decoupled frequency-response representations are satisfactory descriptions of large motion helicopter dynamics in hover and forward flight.

7. OBTAINING GOOD FREQUENCY-RESPONSE IDENTIFICATION RESULTS

This section reviews piloting and analysis aspects which are important for obtaining good frequency-response identification results. The comments and suggestions presented in the following sections are based on experience gained in this and other similar frequency-sweep tests (refs. 7,8,10-12).

7.1 Flight-Test Technique

The following aspects are important for achieving flight data which yield good frequency-response identification:

1. The sweep input must be initiated from a steady trim condition (in minimum winds, $V_a < 5$ knots), and must conclude in a steady trim condition. The recorded data must include a few seconds of this trim at the start and end of each sweep.

2. Input in the off-axes.

   (a) Hover. Lateral stick inputs may cause significant coupling to the directional axis. Heading excursions should be reduced (to roughly ±20 deg) with pedal inputs. This should be considered as a low-frequency and low-priority piloting function. Similarly, power lever inputs should be used to avoid large height excursions during longitudinal sweeps.

   (b) Forward flight. Lateral stick inputs will cause sideslip excursions. Pedals should not be used during lateral sweeps unless sideslip operational limitations are encountered. It is preferable to reduce the magnitude of the lateral inputs if sideslip excursions are too great, rather than to use large pedal inputs.

3. The frequency-sweep input form (shape) should be adjusted during the run to avoid large asymmetrical aircraft response. For example, the "center reference" of the longitudinal sweep should be shifted to maintain a roughly constant "reference (center) airspeed" during each run. However, large shifts in either the reference control position or the reference aircraft state degrade the quality of the data.

7.2 Pilot Comments on Frequency-Sweep Inputs in the Bell 214ST Helicopter

The following recommendations are made:

1. That yaw inputs be performed prior to other inputs since the yaw rates were very low and it will aid in the pilot learning curve. The test should be done in order of increasing difficulty: yaw, collective, longitudinal, and then lateral inputs.

2. That aircraft gross weight be at a minimum during the collective inputs. Maximum gross weight for the Bell 214ST is 17,500 lb and the test was conducted at approximately 13,000 lb. Torque readings were consistently greater than 90% (above 100% constitutes an overtorque).

3. That the pilot be "coached" during the input. It is very easy to remain at one frequency too long; therefore, having the engineer tell the pilot to remain on a specific frequency longer or to increase frequency during a data run aided in data acquisition. This assumes the engineer has real-time data.

4. That the copilot or flight-test engineer coach the pilot for the low-frequency responses by counting seconds for timing the quarter-period. This should only be done for the lowest frequencies. It was found that if the copilot tried counting at the higher frequency, it only confused the pilot and resulted in the pilot following the counting rather than increasing the frequency as required by the test.

5. That pilots practice the inputs utilizing an external power supply (hydraulic and electrical power) on the ground prior to testing. This should significantly reduce flight-test time.

6. A "scope" with "freeze" capability be installed in the test aircraft unless "real-time" TM is available.

7. That the test team be briefed on all "aircraft" natural frequencies below 4.0 Hz and any resultant problems which may be encountered at these frequencies.

8. During flights that require longitudinal inputs, the instrumented A/S boom must be monitored closely for deflection beyond limits or removed.

7.3 Safety of Flight Considerations

Experience in this and other flight tests shows that frequency-sweep testing involves much smaller response excursions and loads than are encountered in standard controllability test programs (involving steps, pulses, etc.). The largest attitude excursions occur during the low-frequency inputs at the beginning of the run; these excursions generally do not exceed ±10 deg (pitch or roll). The maximum angular rates generally do not exceed ±20 deg/sec, and the maximum stick deflections generally do not exceed ±20%. However, the operational limits of a specific test aircraft must be reviewed and maximum excursions established before the flight tests commence.

It is necessary for the flight crew and test engineer to be familiar with the dominant rotor and fuselage modal frequencies. If the excitation of these modes is excessive, the frequency-sweeps should be terminated before the higher frequencies are achieved. The slow progression of input frequencies during the frequency-sweeps makes it easy for the flight-test engineer (who is monitoring the TM data) to advise the pilot in real time to terminate a run when the maximum desired frequency is reached.

It is desirable that data be taken at input frequencies as high as possible for purposes of specification-compliance testing.

7.4 Frequency-Response Analysis Considerations

Success in achieving good frequency-response identification depends, to a large extent, on the computational tools which are available to the analyst. Most commercially available data-processing packages, such as $MATRIX_x$ (ref. 14), Control-C (ref. 15), and IMSL (ref. 16), provide facilities to compute Fast Fourier Transforms (FFT). However, if the FFT algorithm is applied directly to the raw data without pre- or post-processing, the extracted frequency responses will generally be unsuitable quality. Frequency-response identification requires, at a minimum, the following important processing steps:

28

1. Multiple runs (at least two) of 90 sec duration are necessary to provide sufficient time-history data for accurate frequency-response identification. Each run is preprocessed to remove biases and linear drifts, and then processed <u>individually</u> to determine its coherence function. The highest quality runs are then concatenated and processed together. These long concatenated records allow for sufficient averaging to reduce the effect of noise in the data.

2. The digitized time-history data must be processed with digital filters having break frequencies of less than 1/4 of the sample rate. This removes the effect of digital sample skewing, which otherwise can cause distortions at lower frequency.

3. Data windowing is essential to provide accurate frequency-response identification. The windows must be tapered (for example, in the cosine window, see ref. 17), to prevent "leakage" and reduce "side-lobes" in the spectral analysis. Windows should be overlapped by 50% to obtain maximum averaging and reduce the effects of noise. The window length controls the frequency content in the identification. For the present study, a window length of T_w = 30 sec was used for the roll, pitch, and yaw axis identification; a T_w = 60 sec window was used in the heave axis to improve the low-frequency identification. These window lengths, combined with the concatenated run length of approximately 180 sec, result in a significant amount of data averaging which is a key source of the smooth identified frequency responses obtained in this study. The window length should be adjusted to achieve a good compromise in the coherence at the low- and high-frequency ends of the range of concern (eq. 1).

4. Once the data have concatenated, digitally filtered, and windowed, a standard FFT can be used to obtain the frequency responses of the individual segments. However, a much better algorithm is the Chirp-Z Transform (CZT) which has been found to produce high quality results with flight data in a number of studies (refs. 11 and 12).

5. Frequency responses of the sensor filters and stick filters must be <u>precisely known</u> to make corrections for these additional dynamics. If these corrections are not applied, the identified frequency-response will reflect the additional lags in the sensor dynamics which do not exist in the actual vehicle response.

8. CONCLUSIONS

1. Frequency-sweep testing and analysis is a practical method for obtaining frequency responses needed to demonstrate LHX handling-qualities specification compliance.

2. The frequency-sweep technique has been successfully demonstrated on the Bell 214ST helicopter using the following procedure:

(a) Three 90-sec sweeps were to be conducted in each axis and flight condition to obtain sufficient dynamic data for the identification process. Frequency-sweep flight testing required approximately 1 flight hour/flight condition. Pilot training was necessary and required additional flight time.

(b) Frequency sweeps were individually analyzed. The best two (out of three) runs were concatenated in the spectral analysis.

(c) The frequency response identification software used is capable of:
    i.   Concatenation or records
    ii. Digital prefiltering
    iii. Overlap-windowing
    iv. Spectral calculations of:
- input-autospectrum, output-autospectrum and cross-spectrum
- frequency response
- coherence function

    v.   Using the Chirp Z-Transform

(d) Least-squares phase curve fitting is necessary when high-frequency coherence is poor or high-frequency structural modes are present which distort the value of the phase-delay based on the 2-pt definition.

3.   The closed-loop frequency responses of the Bell 214-ST in hover and forward flight are adequately represented by very low-order transfer-function models.

4.   The close agreement between the aircraft responses and model responses for large and varied input forms validates the frequency response and lower-order modeling concepts for conventional single-rotor helicopters.

REFERENCES

1. Hoh, Roger H.; Mitchell, David G.; Ashkenas, Irving L.; Aponso, Bimal L.; Fergusen, Samuel W.; Rosenthal, Theodore J.; Key, David L.; and Blanken, Chris L.; Mission-Oriented Flying Qualities Requirements for Military Rotorcraft, Proposed Specification, NASA TR 1194-2, December 1985.

2. Helicopter Flying and Ground Handling Qualities, General Requirements for, MIL-H-8501A, 1961.

3. Tischler, M. B.: Digital Control of Highly Augmented Combat Rotorcraft, NASA TM 83346, 1987.

4. Hoh, Roger H.; Mitchell, David G.; Ashkenas, Irving L.; Aponso, Bimal L.; Fergusen, Samuel W.; Rosenthal, Theodore J.; Key, David L.; and Blanken, Chris L.: Background Information and User's Guide for Proposed Handling Qualities Requirements for Military Rotorcraft, STI TR R-1194-3, December 1985.

5. Hoh, Roger H.; Ashkenas, I. L.; Rignland, R. F.; and Craig, S.: Development of Handling Quality Criteria for Aircraft with Independent Control of Six Degrees of Freedom, TR-81-3027, Air Force Wright Aero Lab, 1981.

6. Jex, H. R.; Hogue, J. R.; Magdaleno, R. E.; and Gelhausen, P. A.: Dynamic Flight-Tests of the Skyship-500 Airship, TR-1151-4, System Technology, Inc., March 1986.

7. Tischler, M. B.; Leung, J. G. M.; and Dugan, D. C.: Frequency-Domain Identification of XV-15 Tilt-Rotor Aircraft Dynamics in Hovering Flight, AIAA Paper 83-2695, AIAA/AHS 2nd Flight Testing Conference, Las Vegas, November 1983. (Also published in condensed version in J. Amer. Helicopter Soc., vol. 30, no. 2, April 1985, pp. 38-48.)

8. Hilbert, K. B.; Lebacqz, J. V.; and Hindson, W. S.: Flight Investigation of a Multivariable Model-Following Control System for Rotorcraft, AIAA Flight Testing Conference, November 1985.

9. Hogue, J. R.; Jex, H. R.; and Magdaleno, R. E.: Engineering Performance Tests of UH-1 and UH-60 Training Simulator Motion Bases and Visual Systems. Systems Technology, Inc. Working Paper no. 1183-3, Sept. 1982.

10. Tischler, M. B.; Leung, J. G. M.; and Dugan, D. C.: Identification and Verification of Frequency-Domain Models for XV-15 Tilt-Rotor Aircraft Dynamics in Cruising Flight. J. Guid. Control Dyn., vol. 9, no. 4, 1986, pp. 446.

11. Tischler, M. B.: Frequency Response Identification of XV-15 Tilt-Rotor Aircraft Dynamics. NASA TM 89428, 1987. (Also Ph.D. Thesis, Stanford University, Stanford, CA, 1987.)

12. Chen, R. T. N.; and Tischler, M. B.: The Role of Modeling and Flight Testing in Rotorcraft Parameter Identification, 1986 AHS Forum, Washington, DC, June 2-4, 1986.

13. Hoh, Roger H.; Mitchell, David G.; Ashkenas, Irving L.; Heffley, Robert K.; and Hodgkinson, John: Proposed Mil Standard and Handbook--Flying Qualities of Air Vehicles. Vol. II, Proposed MIL Handboodk (AFWAL-TR-82-3081, Systems Technology Incorporated; f33615-80-C-3604), AFWAL-TR-82-3081, 1982.

14. "MATRIX$_x$" User's Guide (Version 5.0), Integrated Systems Inc., Palo Alto, CA, October 1985.

15. CTRL-C, A Language for the Computer-Aided Design of Multivariable Control Systems, User's Guide (2.3), System Control Technology, March 1984.

16. International Mathematical & Statistical Libraries, Inc., Reference Manual, vol. 1, Edition 9, 1982.

17. Bendat, Julius S.; and Pierson, Allen G.: Random Data: Analysis and Measurement Procedures, John Wiley and Sons, Inc., New York, 2nd Ed., 1986.

APPENDIX A

HOVER FLIGHT CONDITION FLIGHT DATA AND RESULTS

LIST OF FIGURES

33

Figure A1.- Lateral stick frequency sweeps.
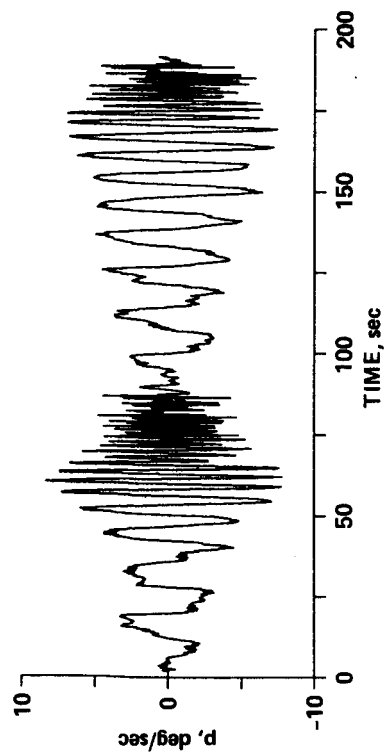

Figure A2.- Lateral stick input autospectrum.

Figure A3.- Roll rate during lateral stick frequency sweeps.
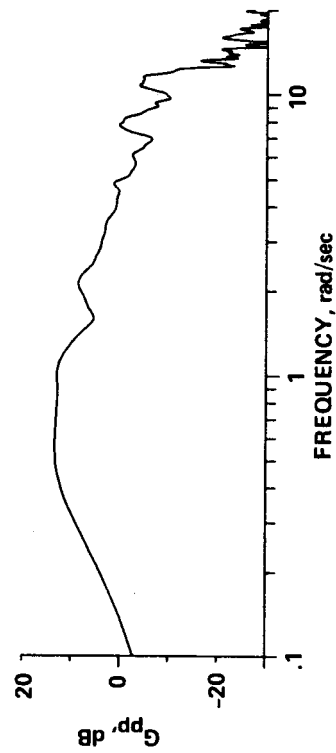

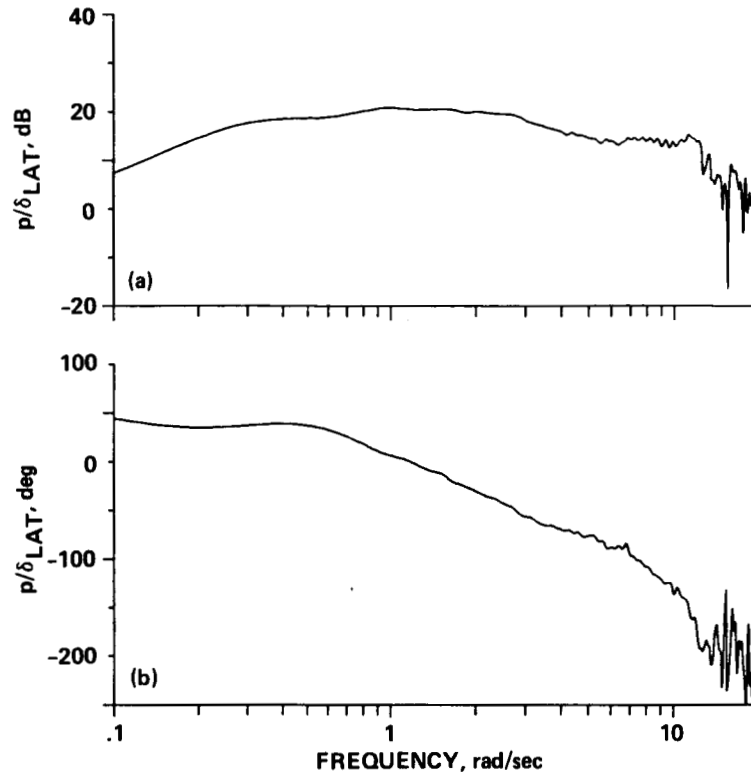Figure A4.- Roll rate output autospectrum.

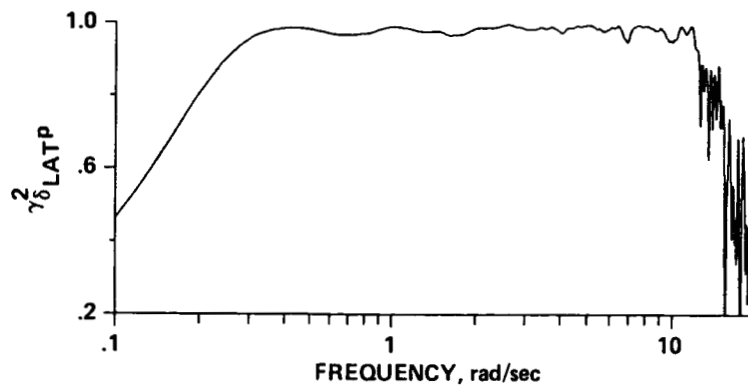Figure A5.- Roll rate response to lateral stick. (a) Magnitude; (b) phase.
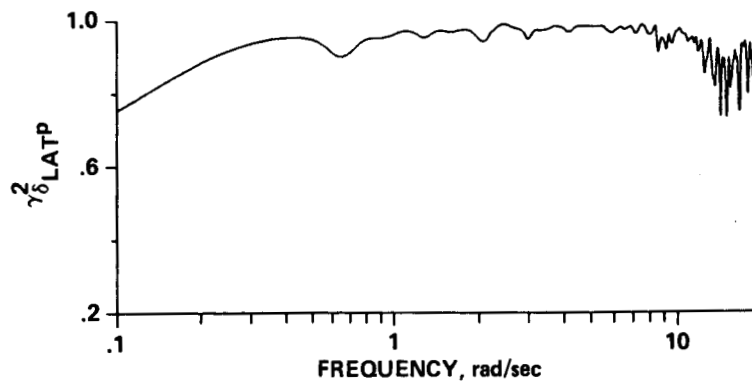
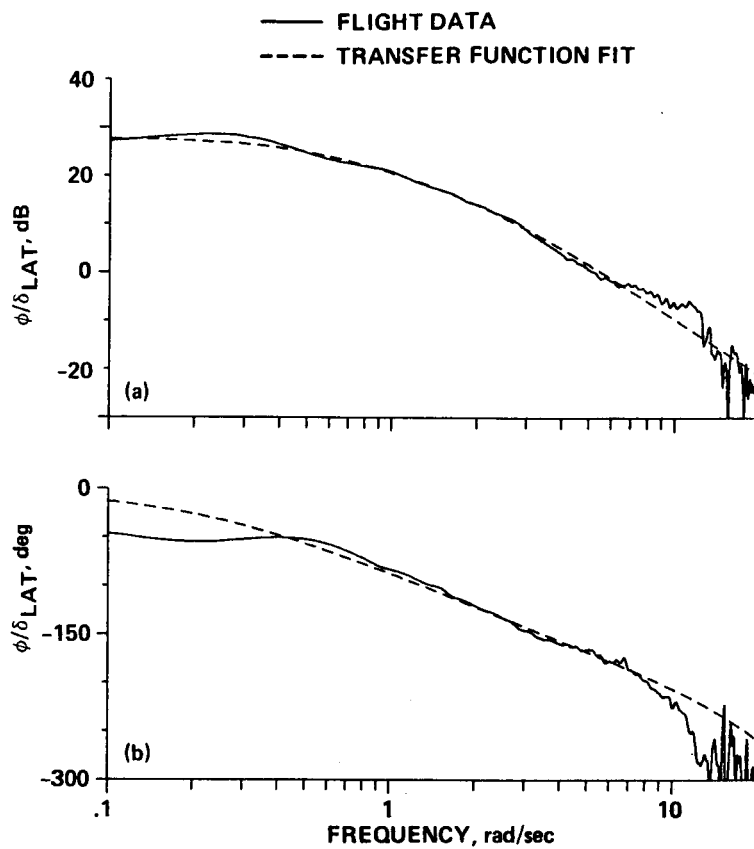Figure A6.- Coherence function for roll rate response to lateral stick.
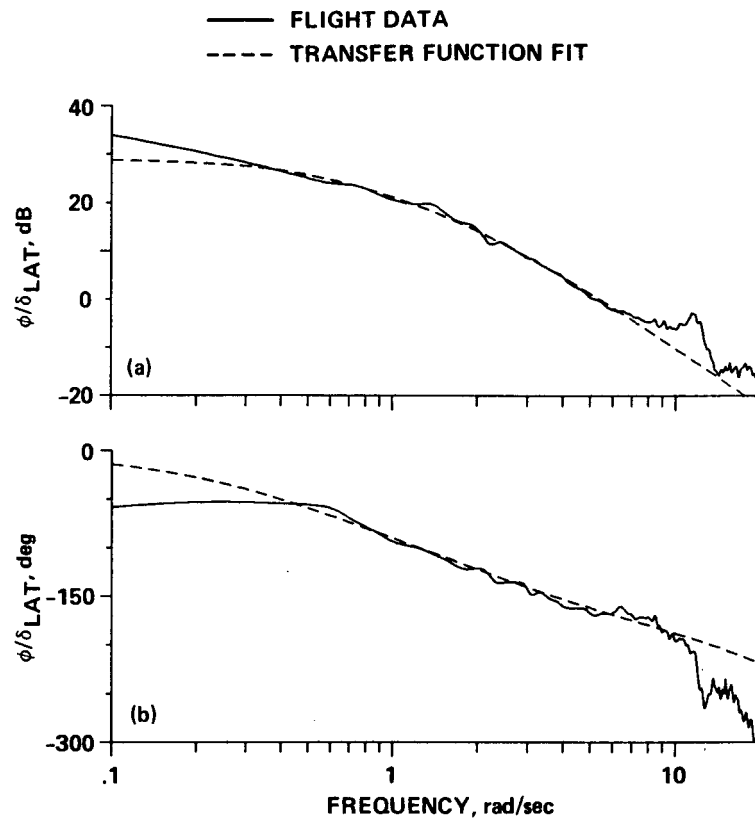
Figure A7.- Transfer function model for roll attitude response to lateral stick. (a) Magnitude; (b) phase.

38
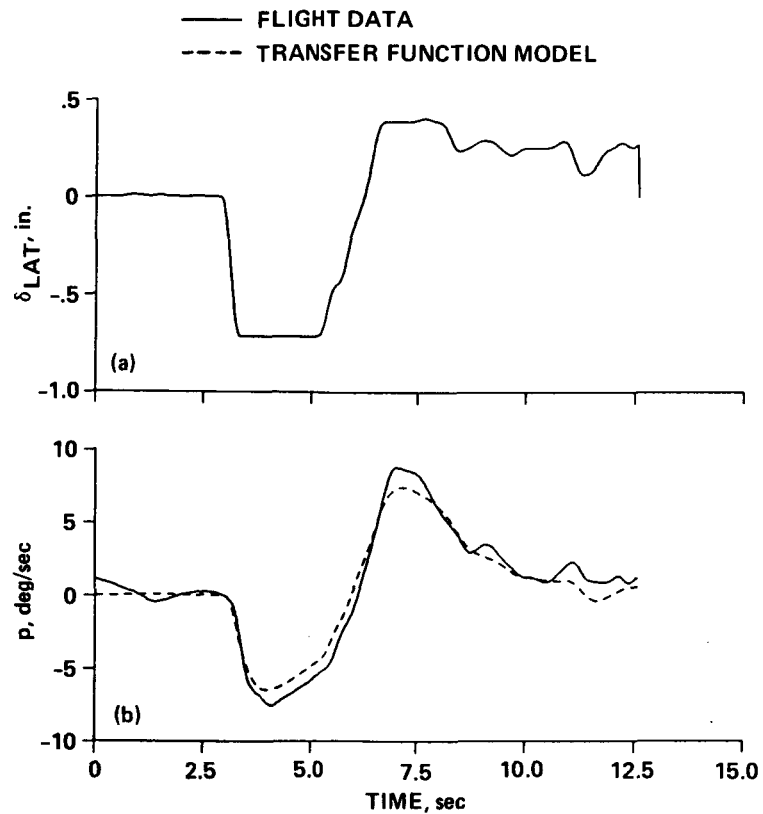
Figure A8.- Comparison of filtered aircraft response and transfer-function model response to a filtered lateral stick step input. (a) Lateral stick input; (b) roll rate.
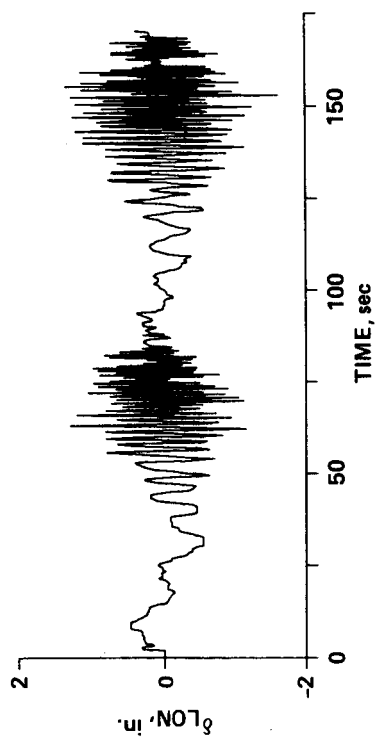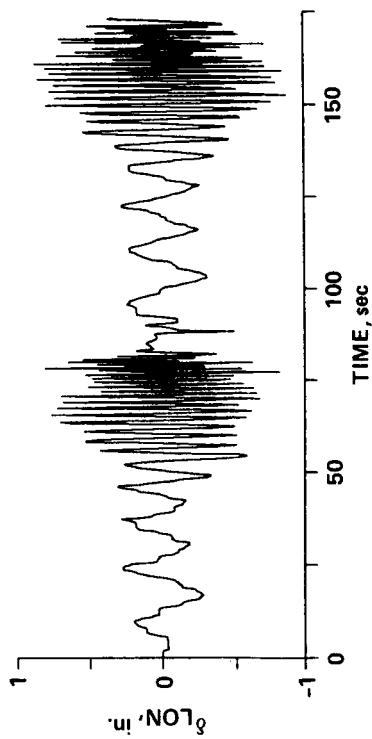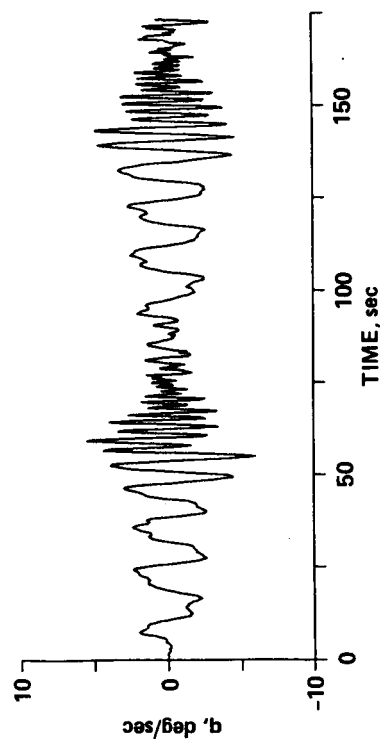
Figure A9.- Longitudinal stick frequency sweeps.
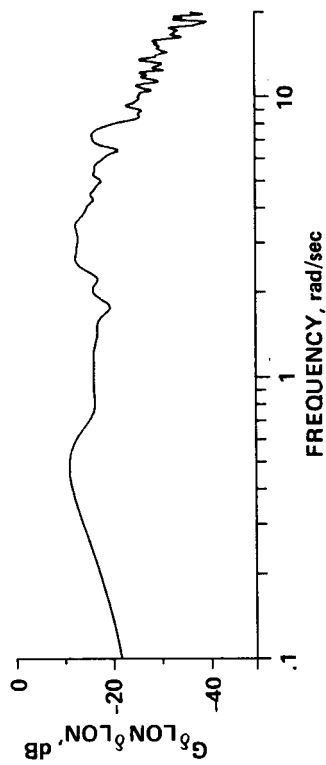

Figure A10.- Longitudinal stick input autospectrum.
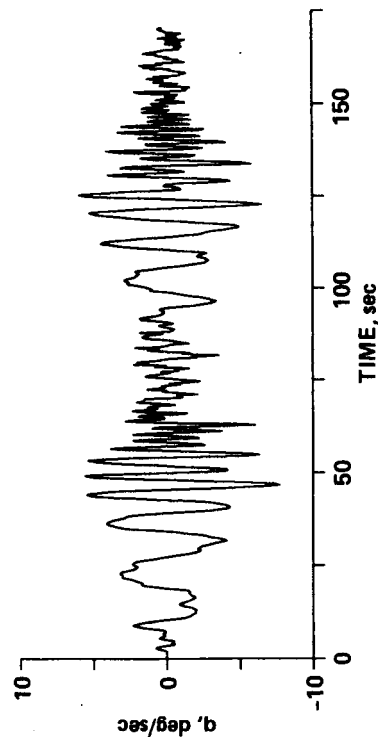
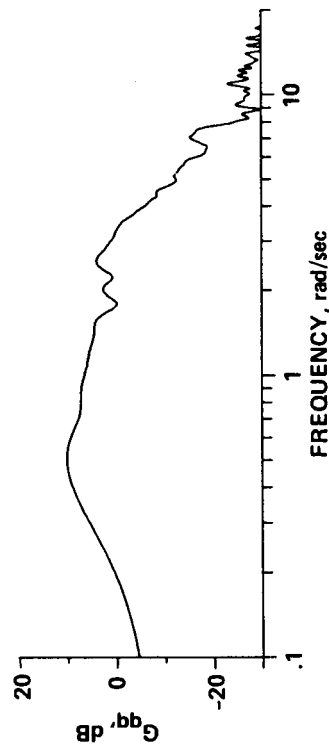Figure A11.- Pitch rate during lateral stick frequency sweeps.
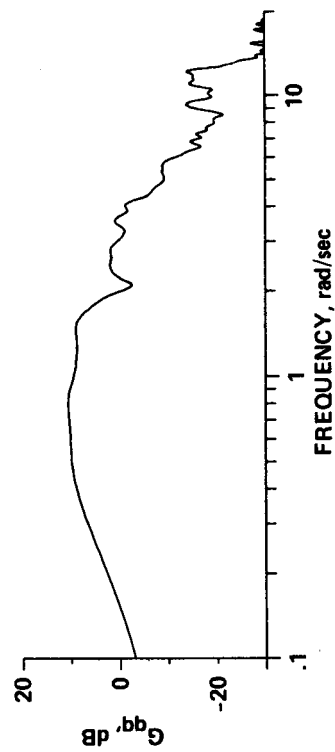
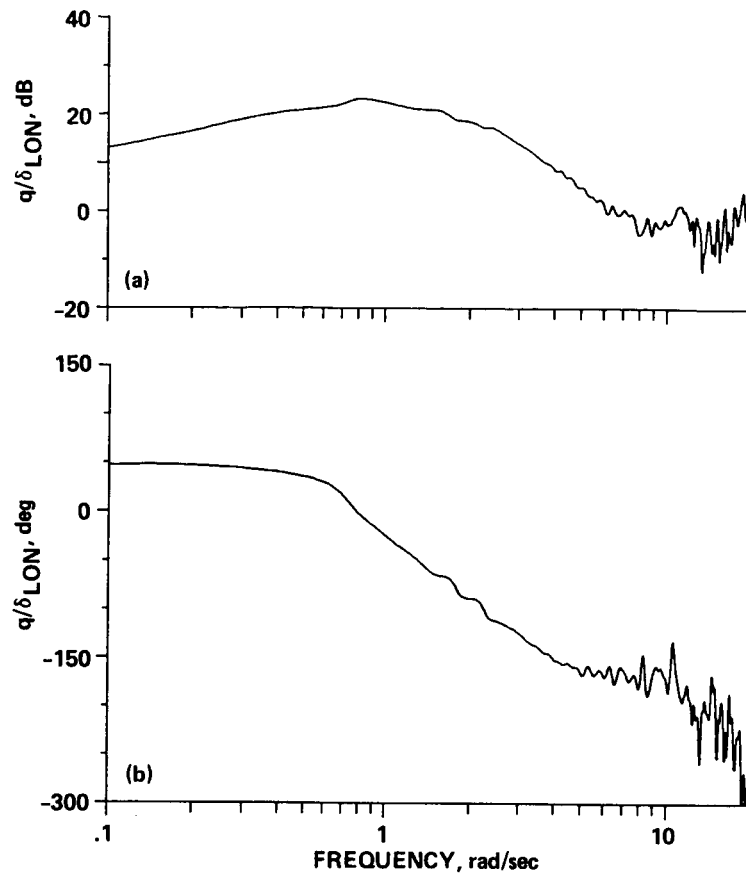

Figure A12.- Pitch rate output autospectrum.
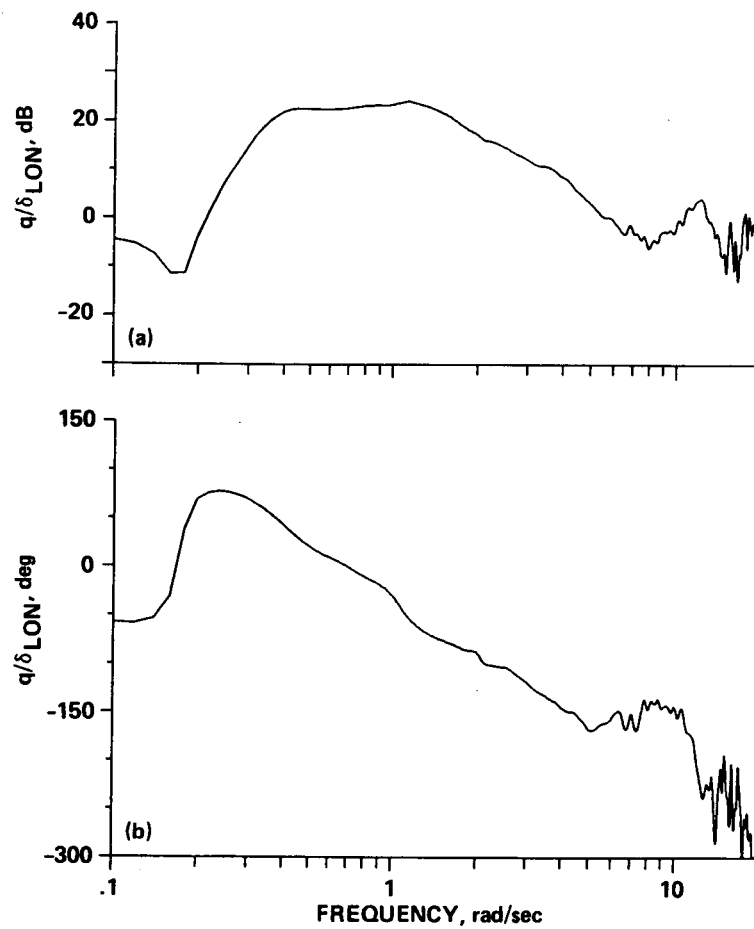
Figure A13.- Pitch rate response to longitudinal stick. (a) Magnitude; (b) phase.
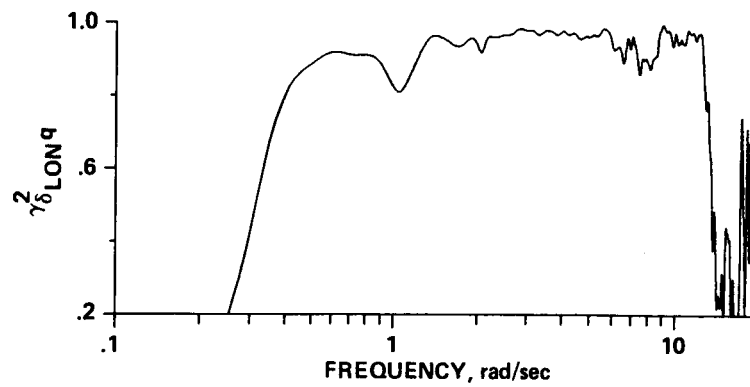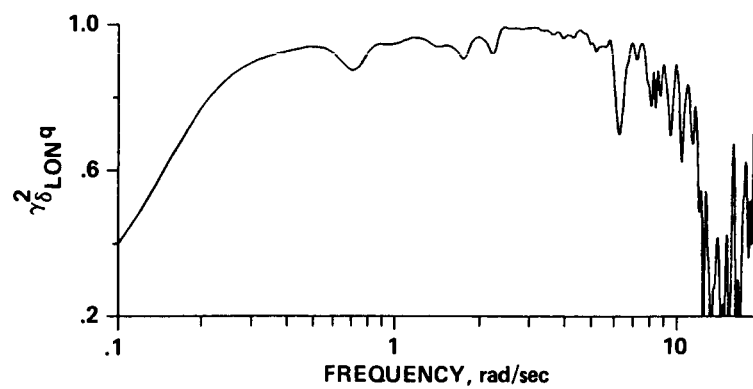

Figure A14.- Coherence function for pitch rate response to longitudinal stick.
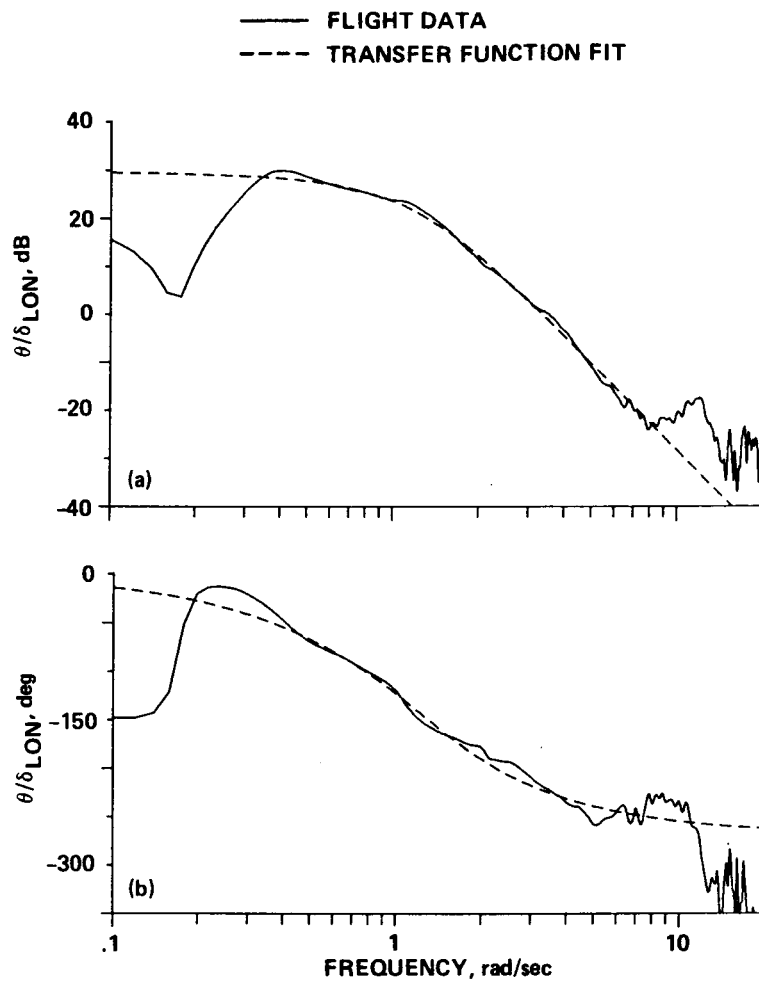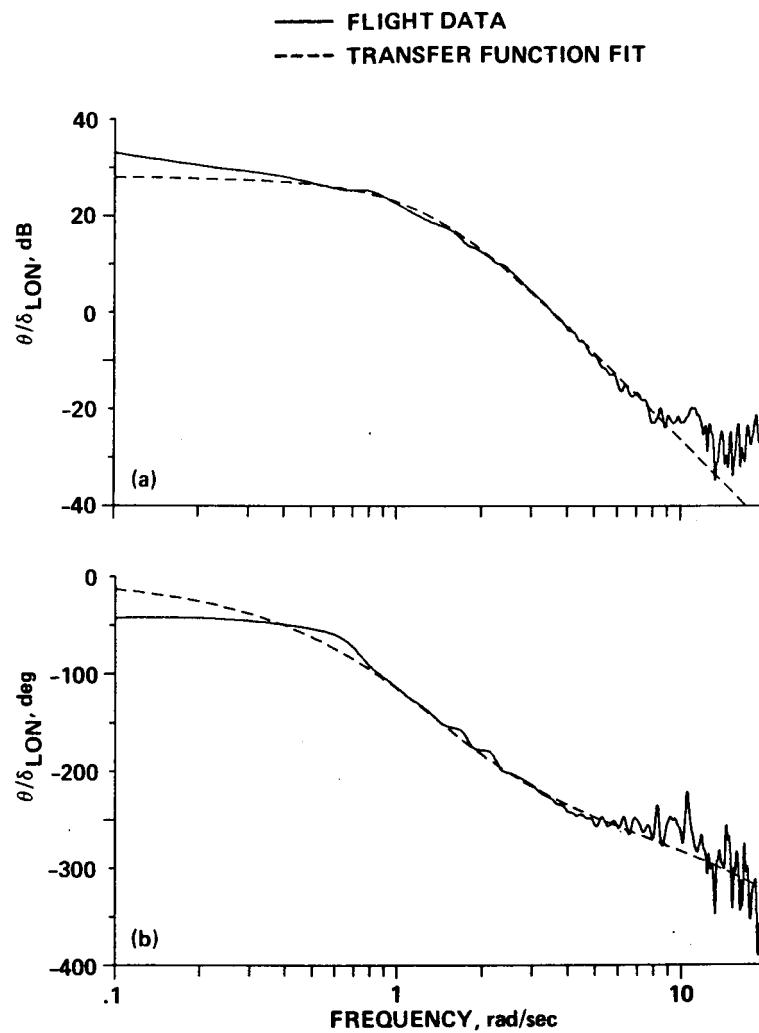
Figure A15.- Transfer function model for pitch attitude response to longitudinal stick. (a) Magnitude; (b) phase.
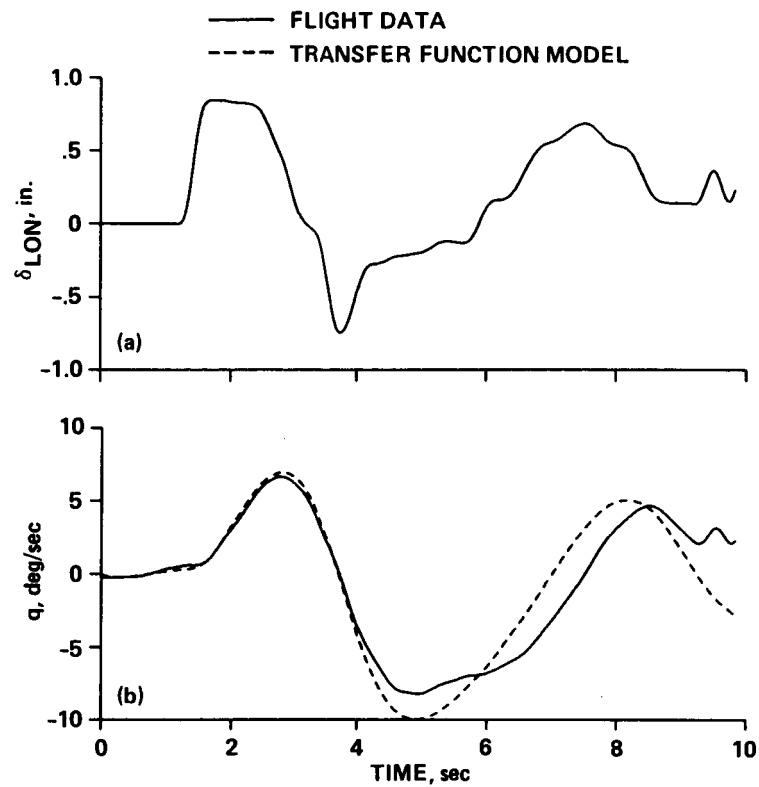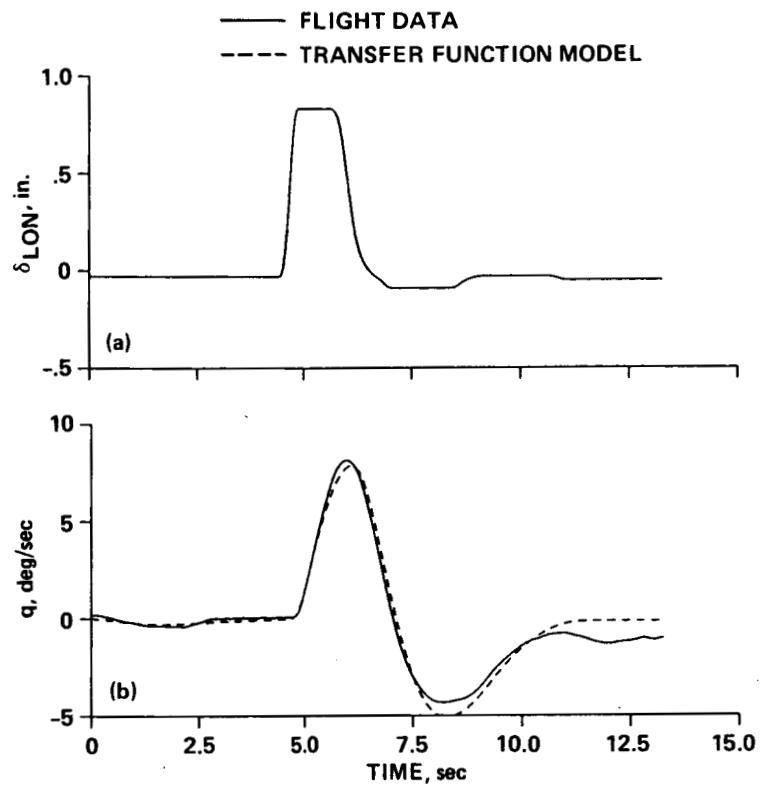
Figure A16.- Comparison of filtered aircraft response and transfer function model response to a filtered longitudinal stick step input. (a) Longitudinal stick input; (b) pitch rate.
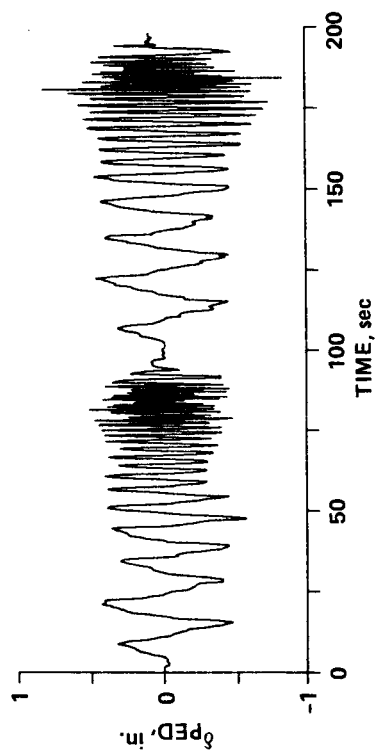
Figure A18.- Pedals input autospectrum.

Figure A20.- Yaw rate output autospectrum.
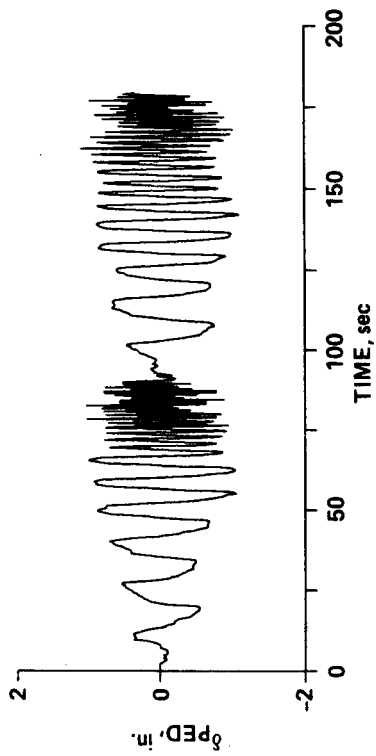
Figure A17.- Pedals frequency sweeps.
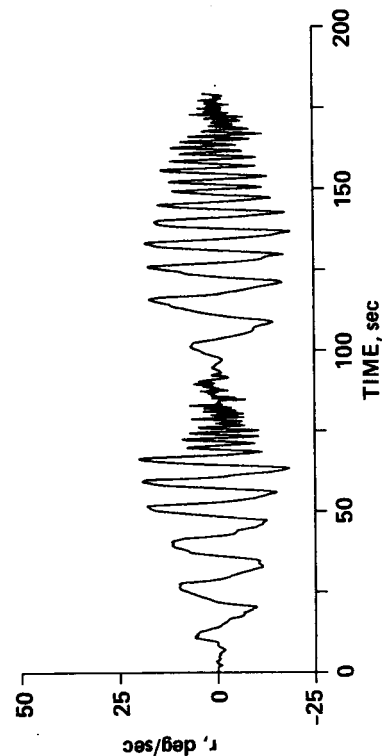
Figure A19.- Yaw rate during pedal frequency
sweep.

44
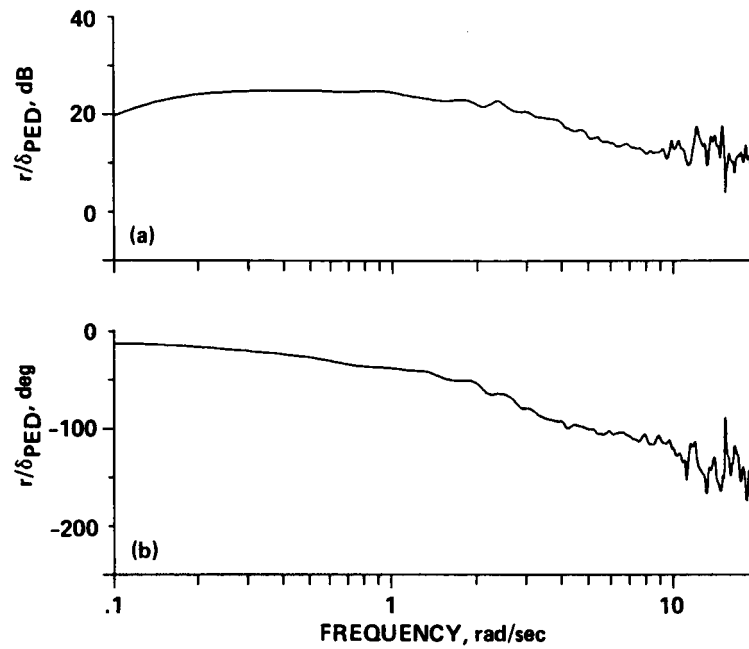
Figure A21.- Yaw rate response to pedals. (a) Magnitude; (b) phase.
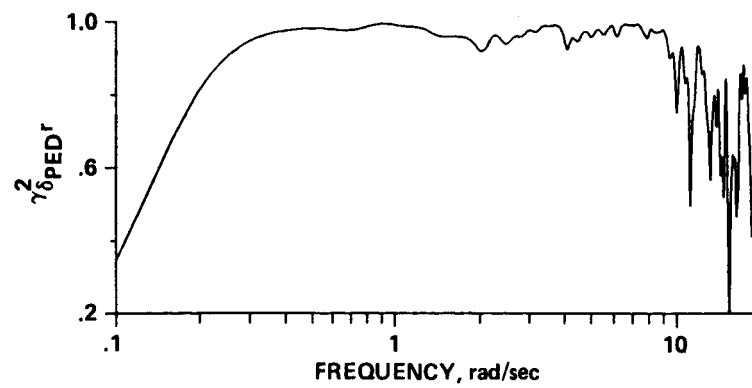
Figure A22.- Coherence function for yaw rate response to pedals.
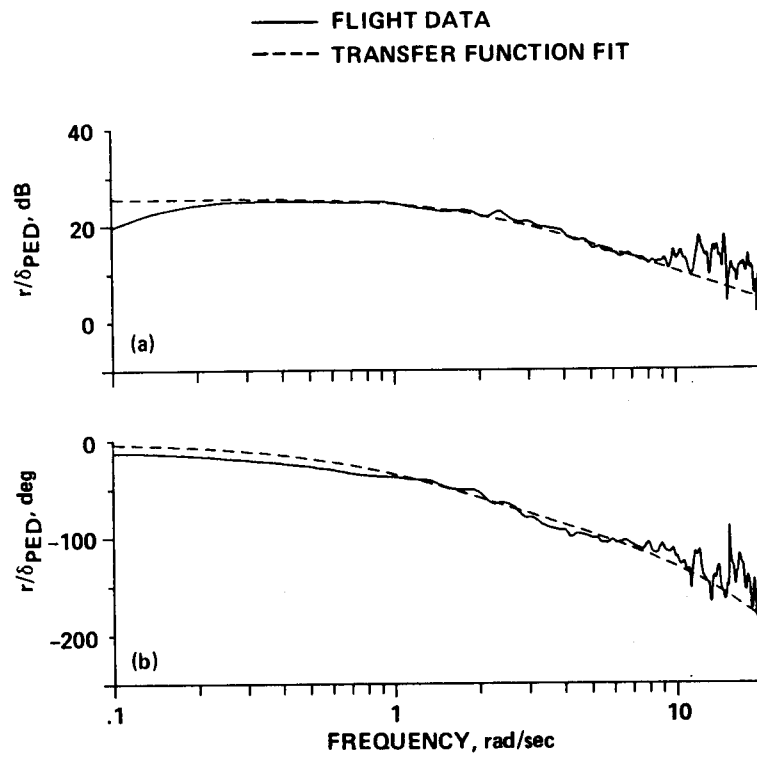
Figure A23.- Transfer function model for yaw rate response to pedals. (a) Magnitude; (b) phase.
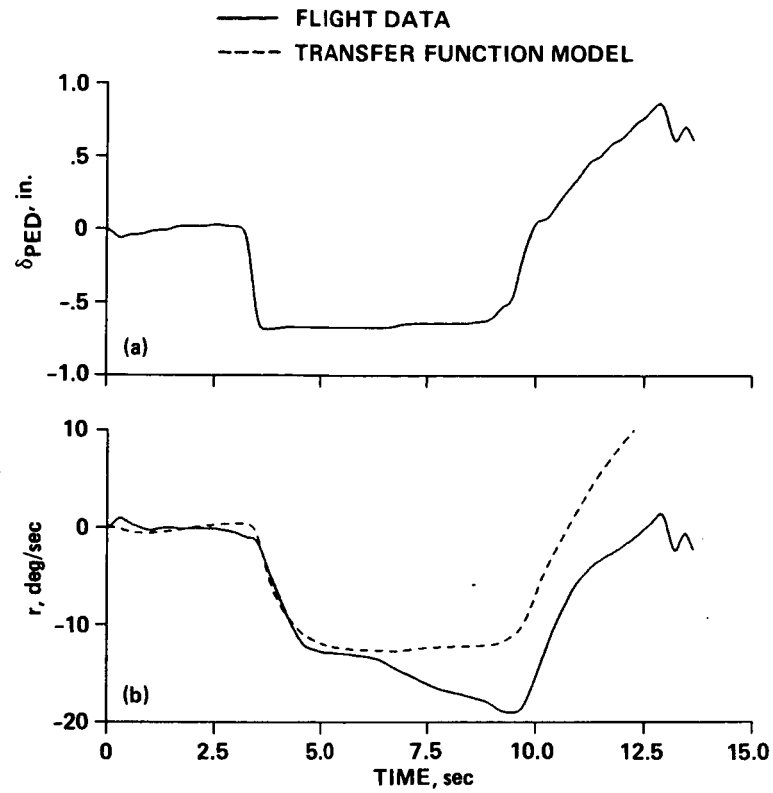
Figure A24.- Comparison of filtered aircraft response and transfer-function model response to a filtered pedals step input. (a) Pedal input; (b) yaw rate.
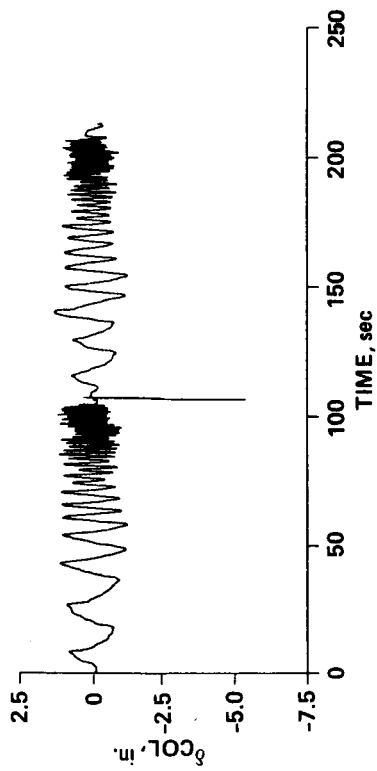
Figure A25.- Collective stick frequency sweeps.

Figure A26.- Collective stick input autospectrum.
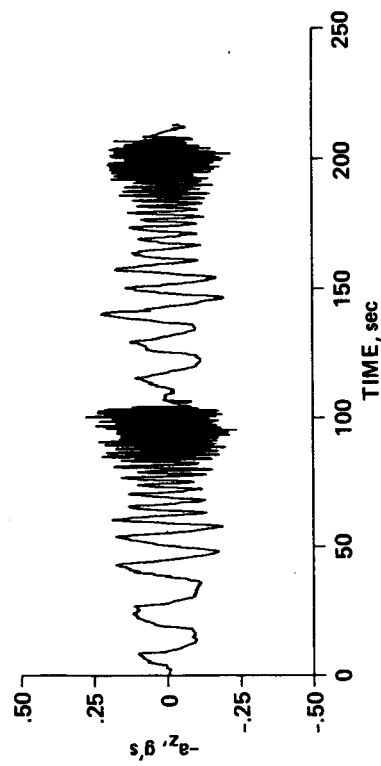
Figure A27.- Vertical acceleration during collective frequency sweeps.
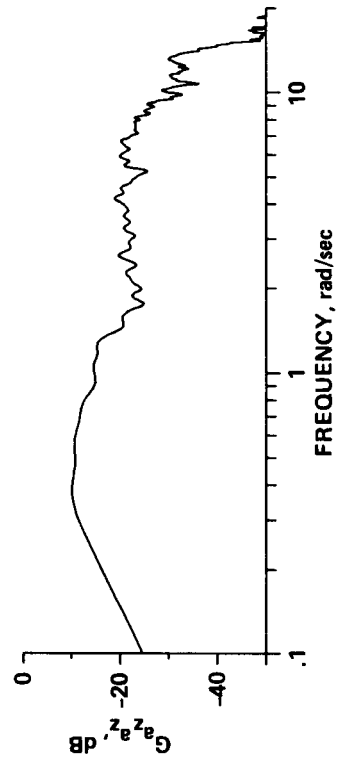
Figure A28.- Vertical acceleration output autospectrum.

48
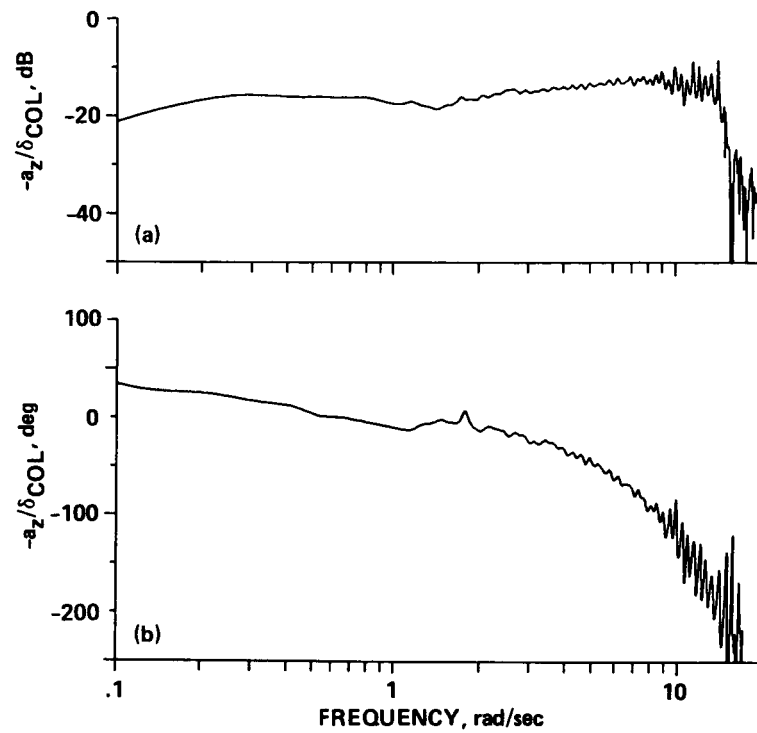
Figure A29.- Vertical acceleration response to collective stick. (a) Magnitude; (b) phase.
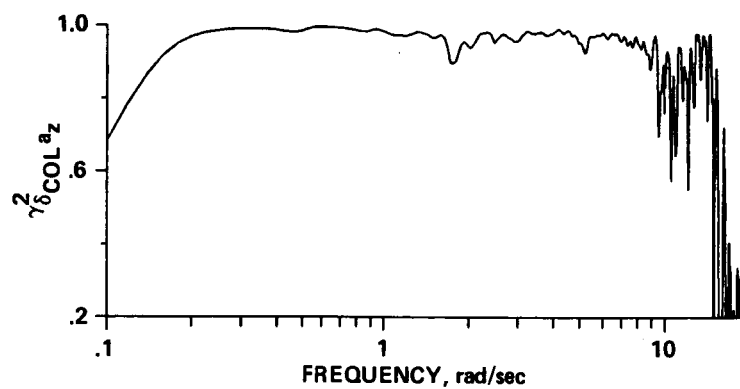
Figure A30.- Coherence function for vertical acceleration response to collective stick.
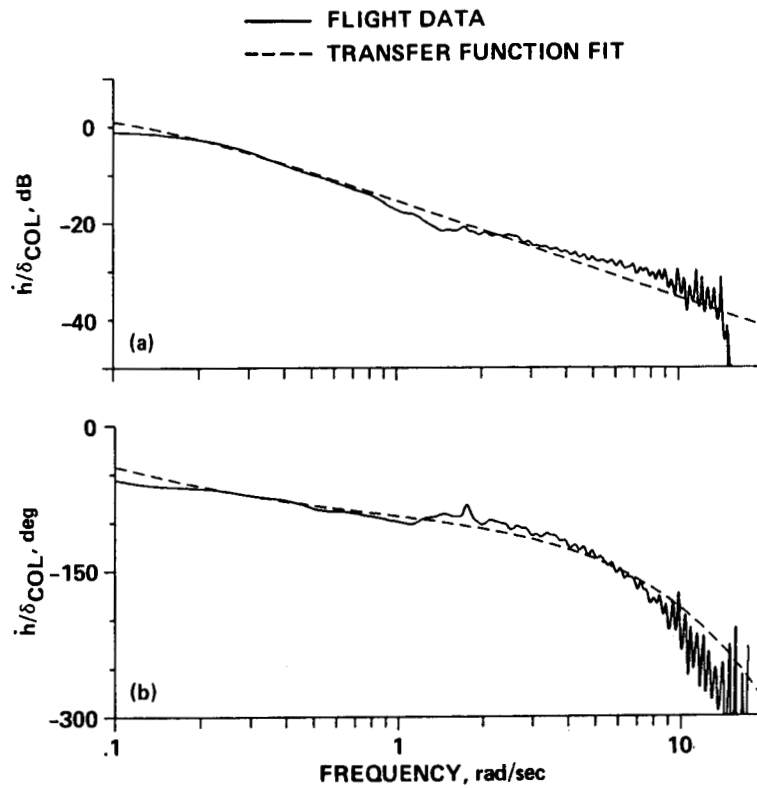
Figure A31.- Transfer function model for vertical velocity response to collective stick. (a) Magnitude; (b) phase.
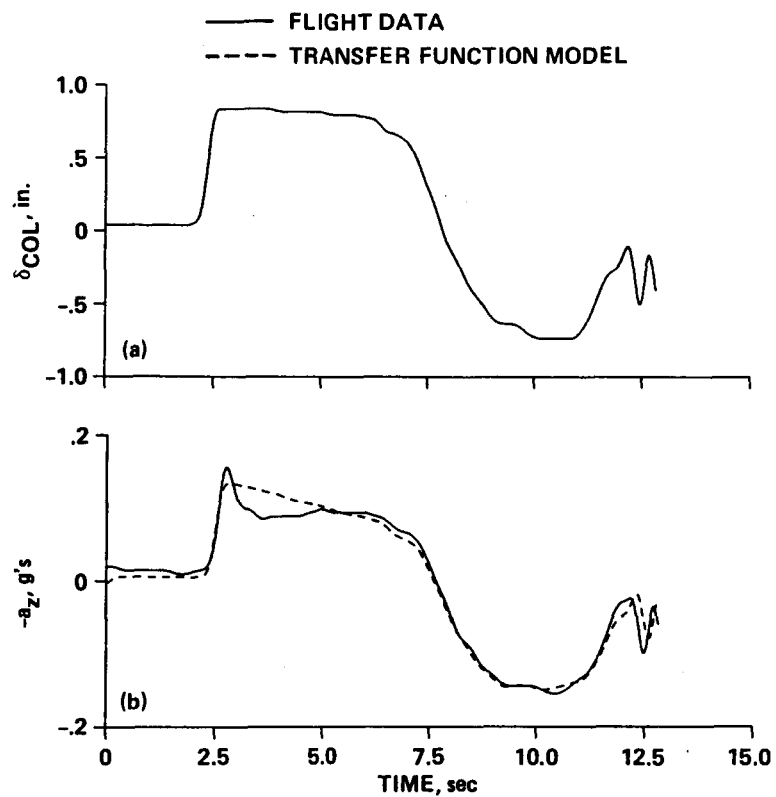
Figure A32.- Comparison of filtered aircraft response and transfer-function model
response to a filtered collective stick step input. (a) Collective stick input;
(b) vertical acceleration.
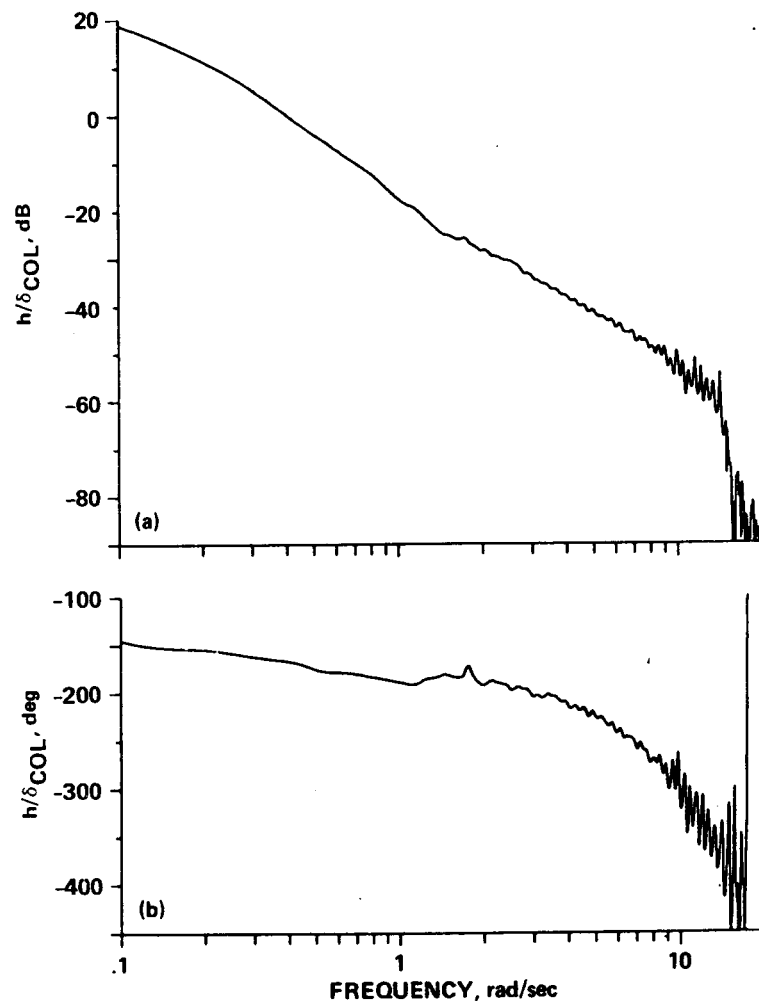
Figure A33.- Vertical position response to collective stick. (a) Magnitude;
(b) phase.

APPENDIX B

LEVEL FLIGHT CONDITION FLIGHT DATA AND RESULTS

LIST OF FIGURES

Figure   Page

Roll Axis

Pitch Axis

53

Heave Axis
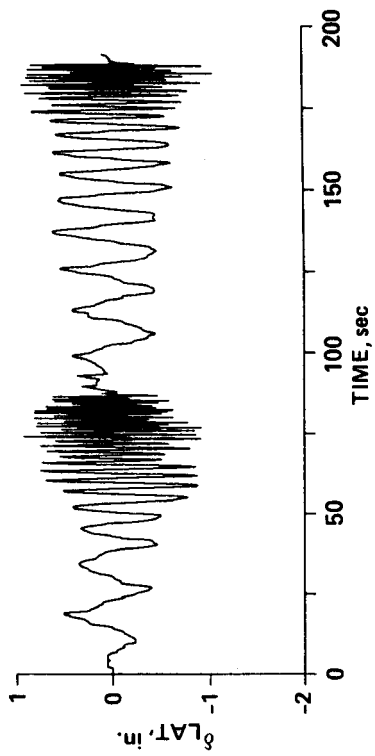
Figure B1.- Lateral stick frequency sweeps.
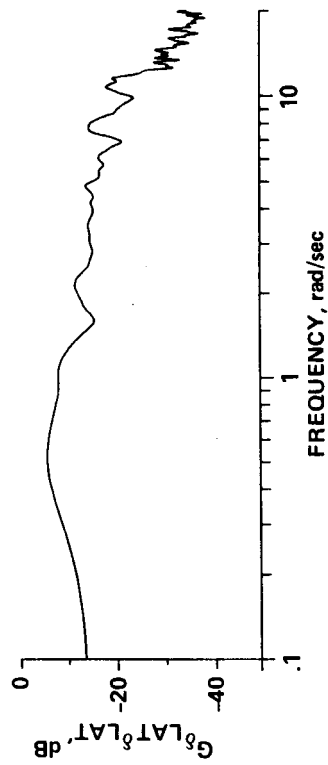
Figure B2.- Lateral stick input autospectrum.

Figure B3.- Roll rate during lateral stick frequency sweeps.

Figure B4.- Roll rate output autospectrum.

Figure B5.- Roll rate response to lateral stick. (a) Magnitude; (b) phase.

Figure B6.- Coherence function for roll rate response to lateral stick.

Figure B7.- Transfer function model for roll attitude response to lateral stick. (a) Magnitude; (b) phase.
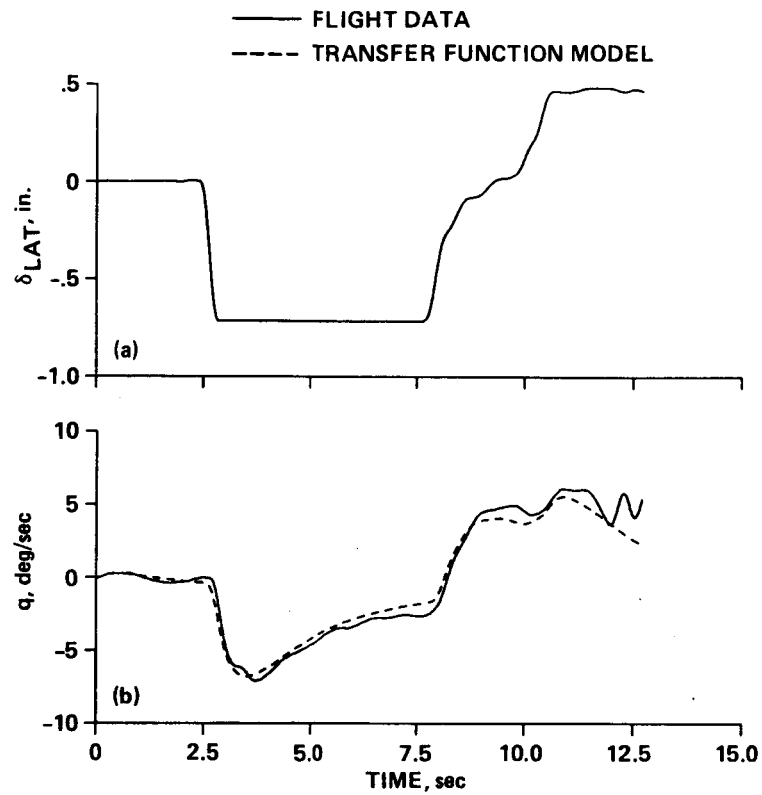
Figure B8.- Comparison of filtered aircraft response and transfer function model response to a filtered lateral stick step input. (a) Lateral stick input; (b) roll rate.

Figure B9.- Longitudinal stick frequency sweeps.

Figure B10.- Longitudinal stick input autospectrum.

Figure B11.- Pitch rate during longitudinal stick frequency sweeps.

Figure B12.- Pitch rate output autospectrum.

Figure B13.- Pitch rate response to longitudinal stick. (a) Magnitude; (b) phase.

Figure B14.- Coherence function for pitch rate response to longitudinal stick.

Figure B15.- Transfer function model for pitch attitude response to longitudinal stick. (a) Magnitude; (b) phase.

Figure B16.- Comparison of filtered aircraft response and transfer function model response to a filtered longitudinal stick step input. (a) Longitudinal stick input; (b) pitch rate.

Figure B17.- Pedal frequency sweeps.
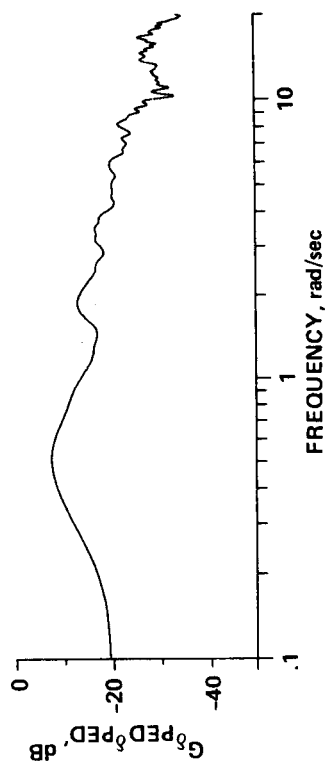
Figure B18.- Pedal input autospectrum.
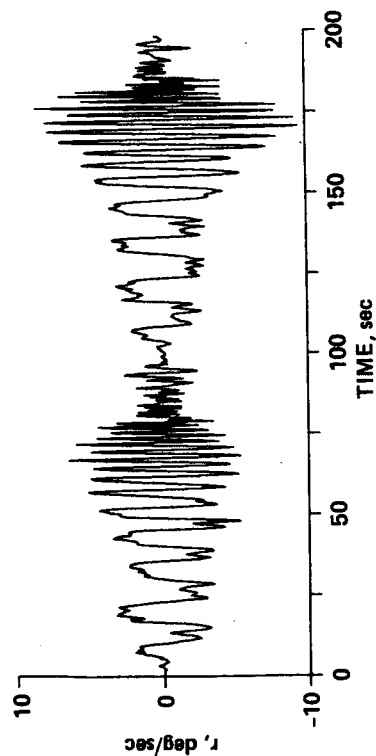
Figure B19.- Yaw rate during pedal input.
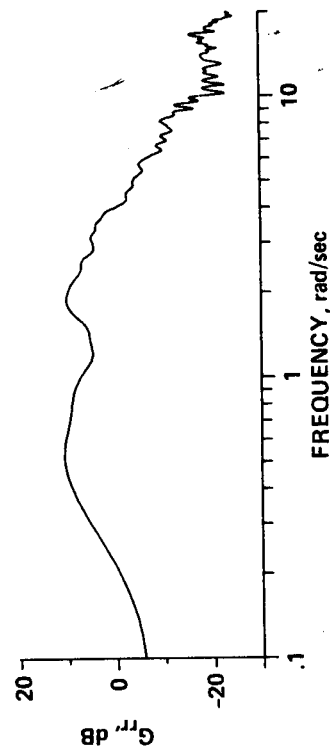
Figure B20.- Yaw rate output autospectrum.

64
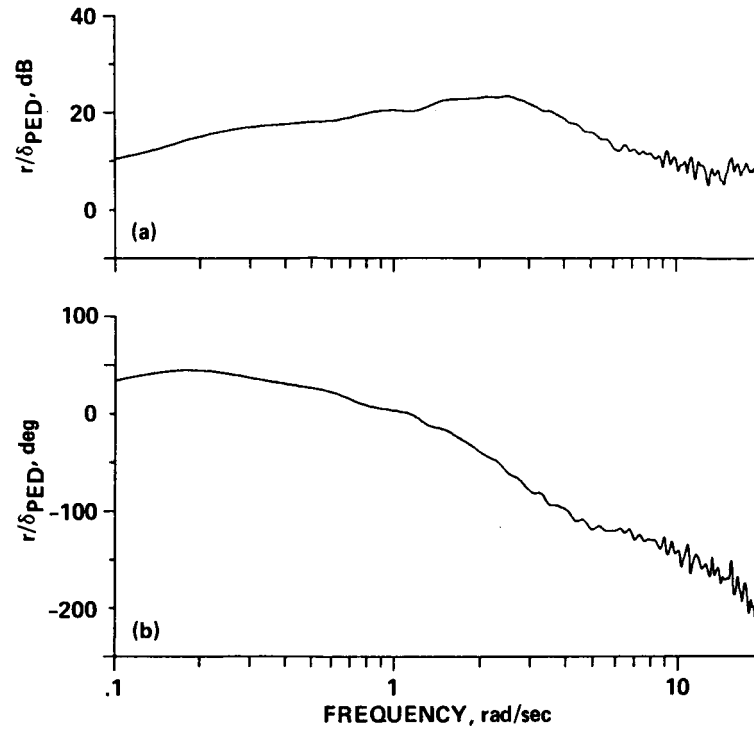
Figure B21.- Yaw rate response to pedals. (a) Magnitude; (b) phase.
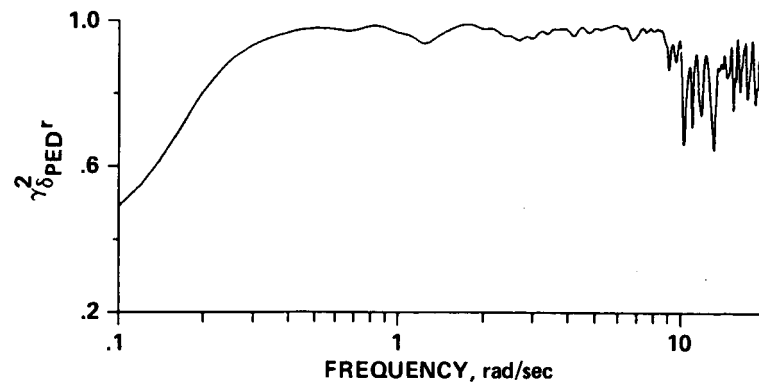
Figure B22.- Coherence function for yaw rate response to pedals.
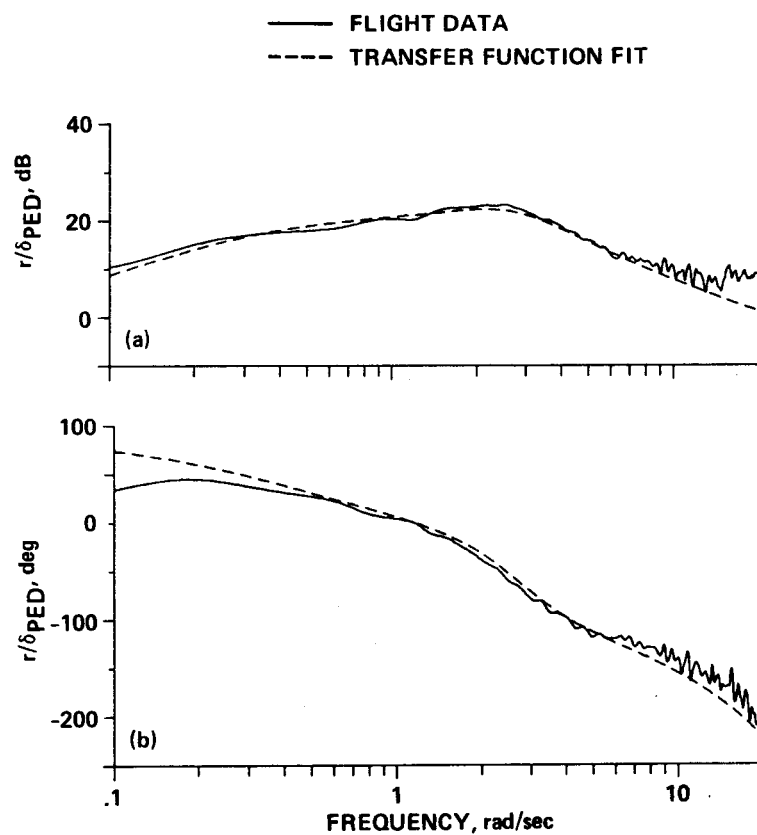
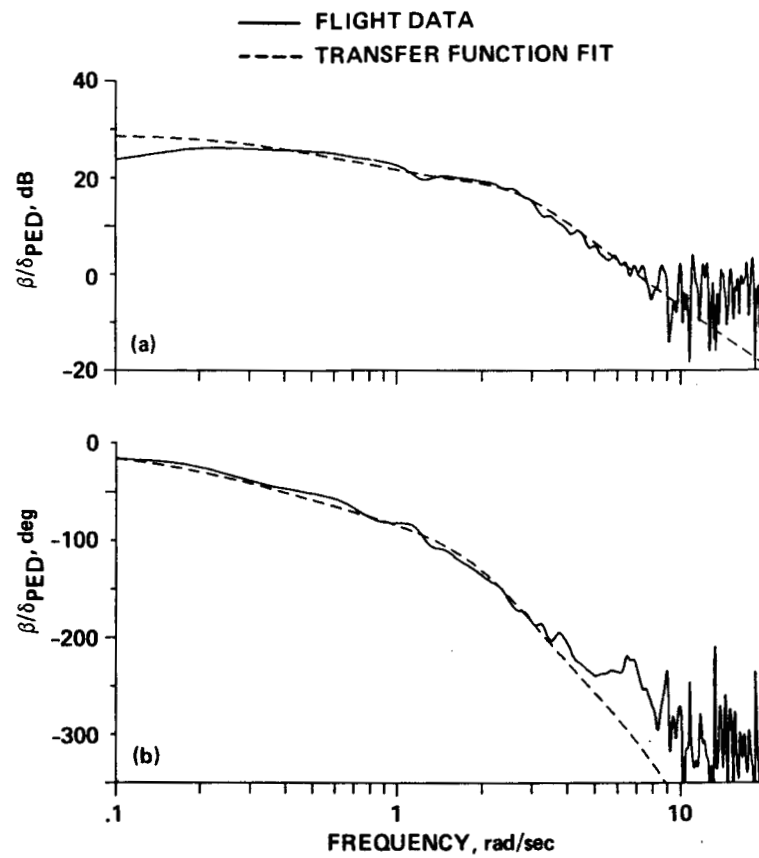Figure B23.- Transfer function model for yaw rate response to pedals.
(a) Magnitude; (b) phase.
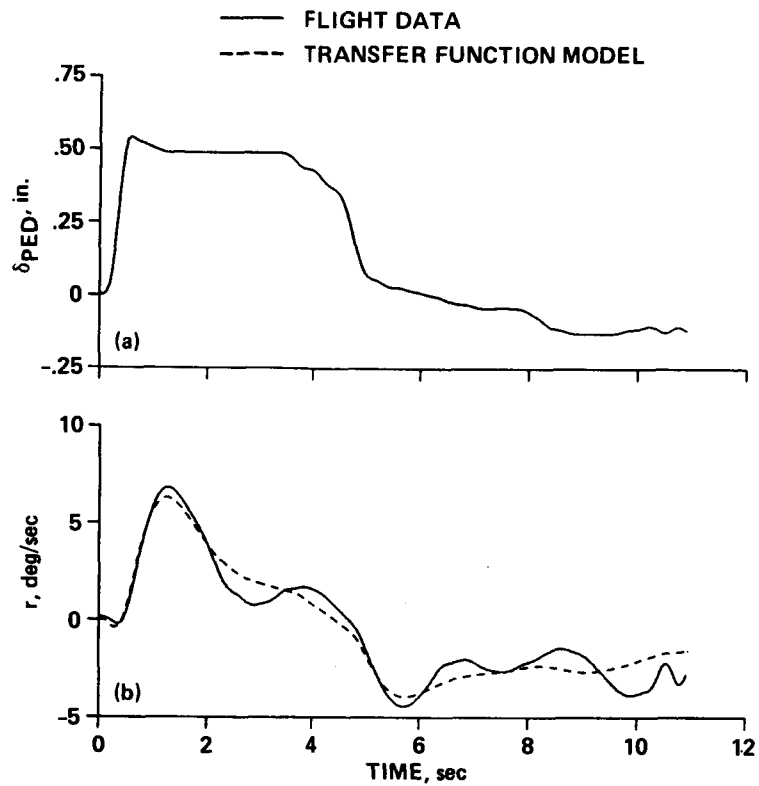
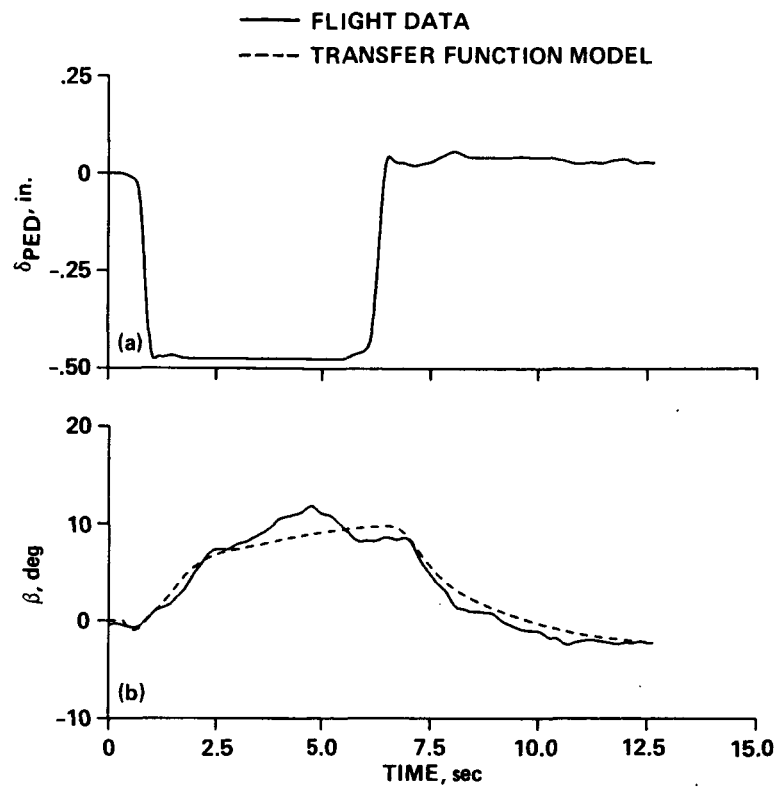Figure B24.- Comparison of filtered aircraft response and transfer function model
response to a filtered pedal step input. (a) Pedal input; (b) yaw rate.
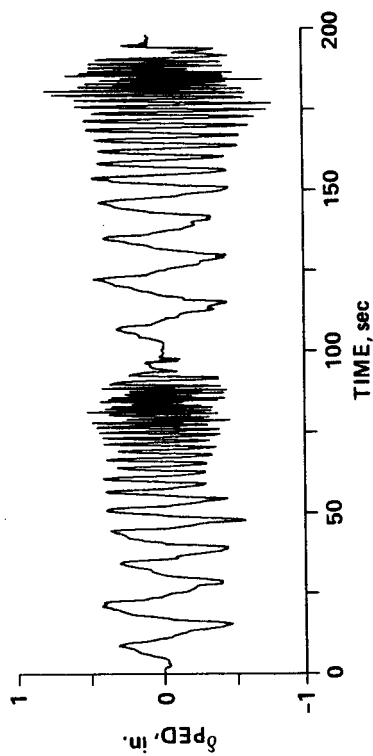
Figure B25.- Pedals frequency sweep.
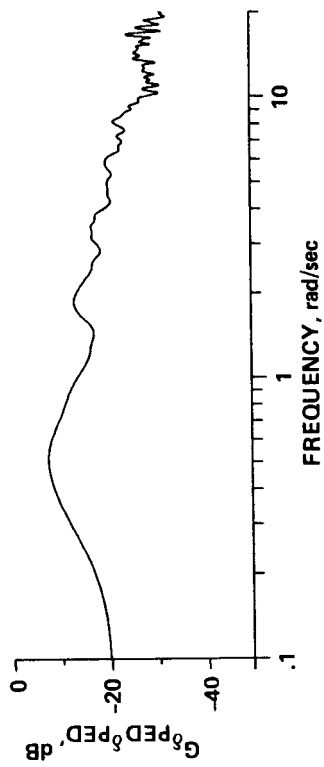
Figure B26.- Pedals input autospectrum.
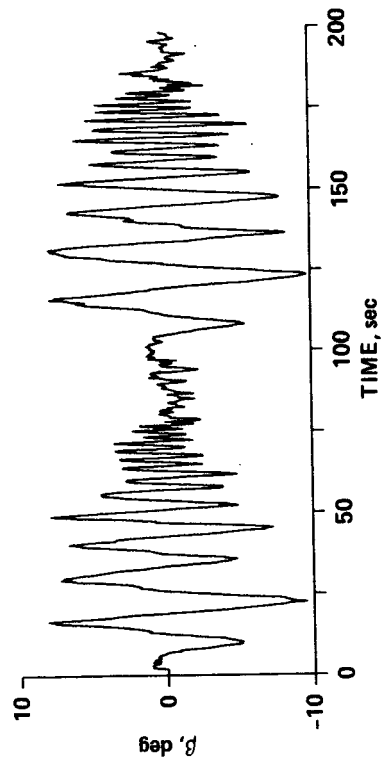
Figure B27.- Side slip angle during pedal inputs.
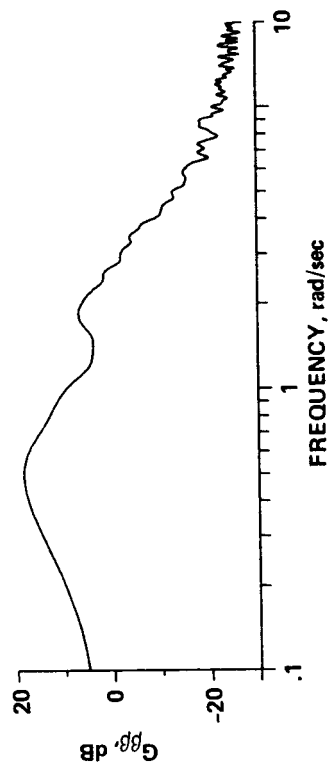
Figure B28.- Side slip angle output autospectrum.

68
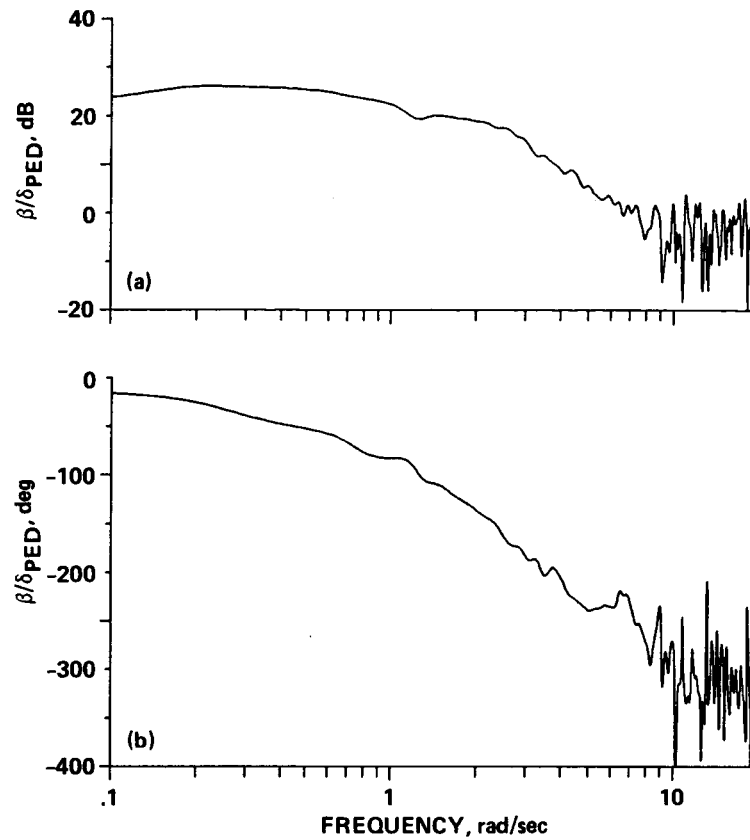
Figure B29.- Side slip angle response to pedals. (a) Magnitude; (b) phase.
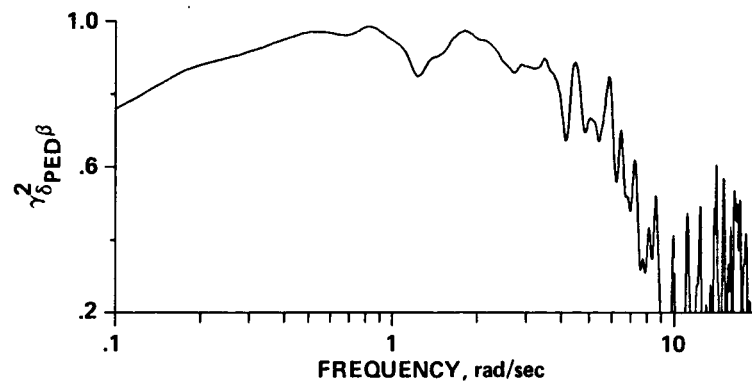
Figure B30.- Coherence function for side slip angle response to pedals.

Figure B31.- Transfer function model for side slip angle response to pedals.
(a) Magnitude; (b) phase.

Figure 32.- Comparison of filtered aircraft response and transfer function model response to a filtered pedals step input. (a) Pedal input; (b) side slip angle.
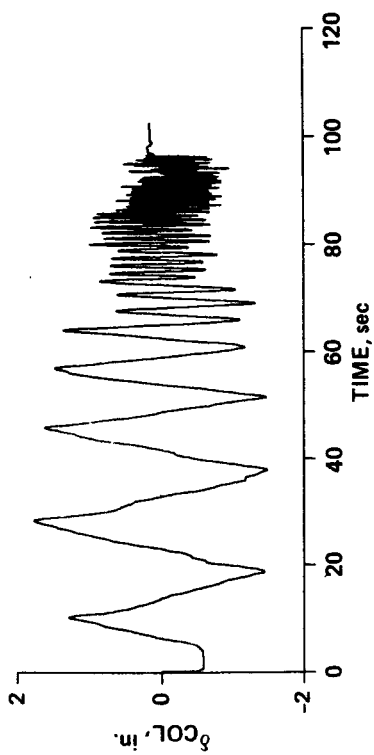
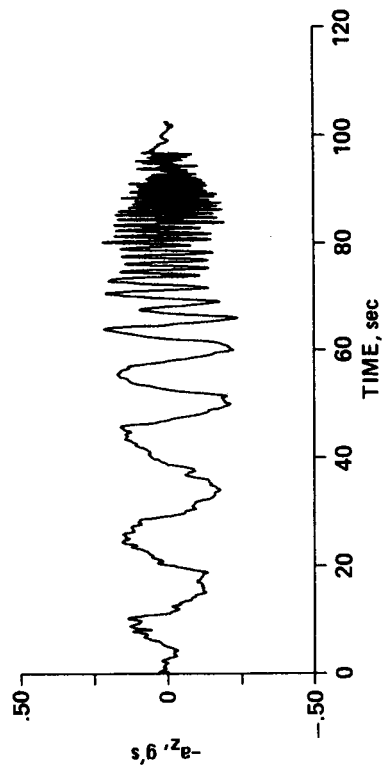Figure B33.- Collective stick frequency sweeps.
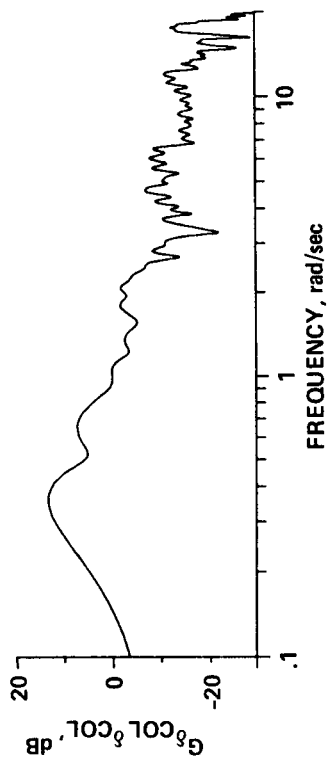
Figure B34.- Collective stick input autospectrum.

Figure B35.- Vertical acceleration during collective stick frequency sweeps.
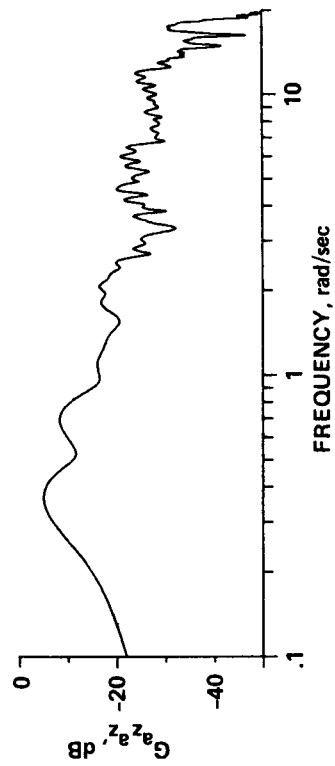

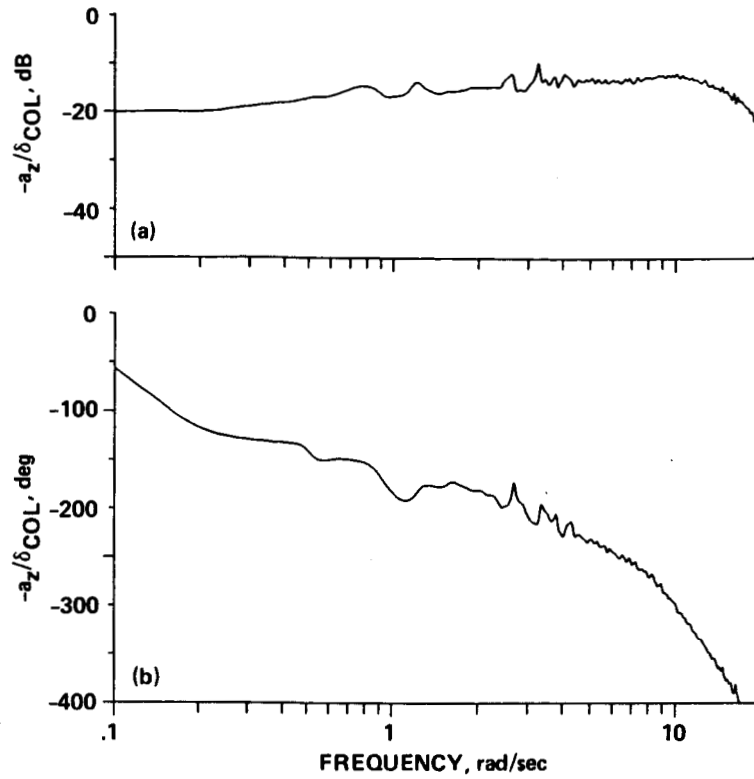Figure B36.- Vertical acceleration output autospectrum.

Figure B37.- Vertical acceleration response to collective stick. (a) Magnitude; (b) phase.
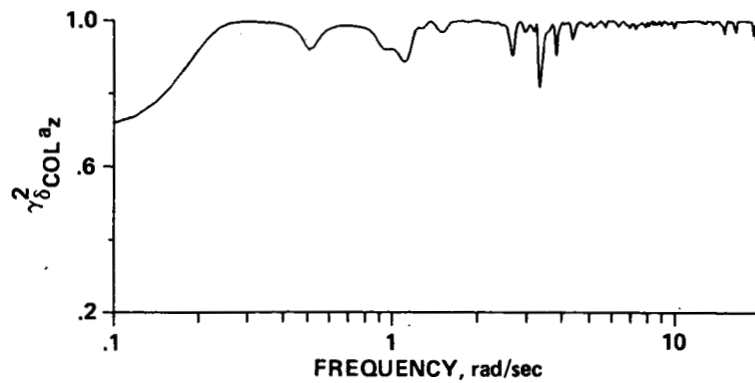

Figure B38.- Coherence function for vertical acceleration response to collective stick.
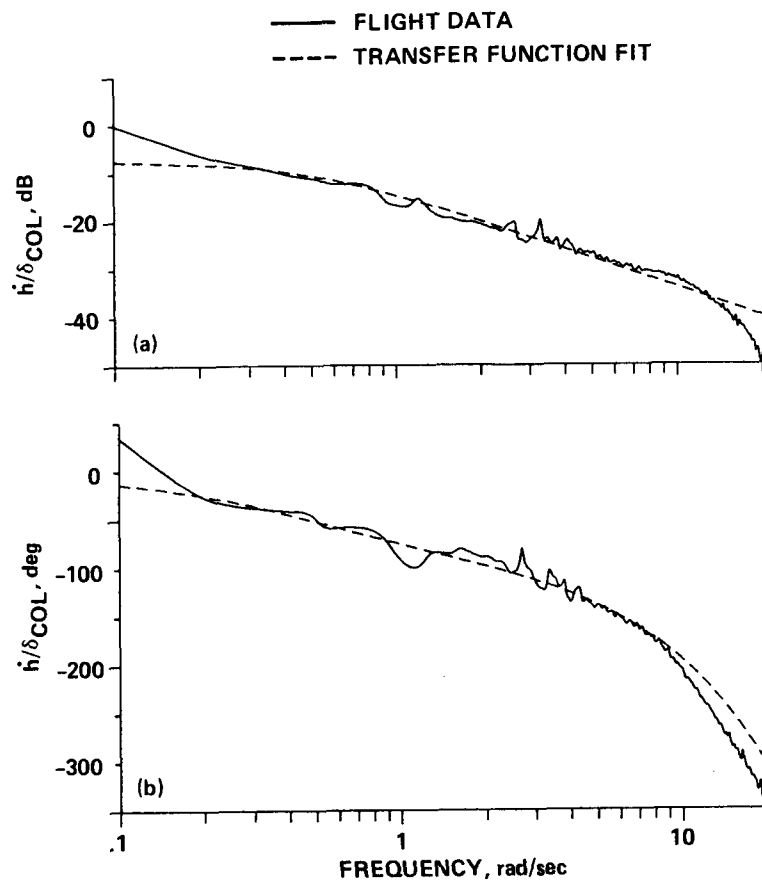
Figure B39.- Transfer function model for vertical velocity response to collective stick. (a) Magnitude; (b) phase.